The germline regulates longevity and somatic repair in a sex-specific manner

Eitan Moses[1,10], Tehila Atlan[1,10], Xue Sun[2], Roman Franek[1,3], Atif Siddiqui[4], Georgi K. Marinov[5], Sagiv Shifman[1], David M. Zucker[6], Adi Oron-Gottesman[1], William J. Greenleaf[5,7,8,9], Ehud Cohen[4], Oren Ram[2], Itamar Harel[1,11]

[1] Department of Genetics, the Silberman Institute, the Hebrew University of Jerusalem, Givat Ram, Jerusalem, 91904, Israel.
[2] Department of Biochemistry, the Silberman Institute, the Hebrew University of Jerusalem, Givat Ram, Jerusalem, 91904, Israel.
[3] University of South Bohemia in Ceske Budejovice, South Bohemian Research Center of Aquaculture and Biodiversity of Hydrocenoses, Vodnany, Czech Republic
[4] Department of Biochemistry and Molecular Biology, the Institute for Medical Research Israel-Canada (IMRIC), the Hebrew University School of Medicine, Jerusalem 91120, Israel
[5] Department of Genetics, Stanford University, Stanford, California 94305, USA
[6] Department of Statistics and Data Science, Hebrew University of Jerusalem, Jerusalem, Israel
[7] Center for Personal Dynamic Regulomes, Stanford University, Stanford, California 94305, USA
[8] Department of Applied Physics, Stanford University, Stanford, California 94305, USA
[9] Chan Zuckerberg Biohub, San Francisco, California, USA
[10] Equal contribution
[11] Corresponding author: itamarh@mail.huji.ac.il

Classical evolutionary theories propose tradeoffs between reproduction, damage repair, and lifespan. However, the specific role of the germline in shaping vertebrate aging remains largely unknown. Here, we use the turquoise killifish (*N. furzeri*) to genetically arrest germline differentiation at discrete stages, and examine how different 'flavors' of infertility impact life-history. We first constructed a comprehensive single-cell gonadal atlas, providing cell-type-specific markers for downstream phenotypic analysis. Next, investigating our genetic models revealed that only germline depletion enhanced female damage repair, while arresting germline differentiation did not. Conversely, germline-depleted males were significantly long-lived, indicating that the mere presence of the germline can negatively affect lifespan. Transcriptomic analysis highlighted enrichment of pro-longevity pathways and genes, with functional conservation in germline-depleted *C. elegans*. Finally, germline depletion extended male healthspan through rejuvenated metabolic functions. Our results suggest that different germline manipulation paradigms can yield pronounced sexually dimorphic phenotypes, implying alternative mechanisms to classical evolutionary tradeoffs.

Introduction

For many species age at maturity is proportional to adult lifespan[1,2]. This correlation has sparked several evolutionary theories invoking a functional trade-off between life-history traits[3–5]. One of the leading concepts, the 'disposable soma' theory, suggests that there is a tradeoff between reproduction, growth, damage repair (e.g. DNA damage), and organismal lifespan[4,6]. Accordingly, a recent study in zebrafish has tested this hypothesis, and proposed that germline repair itself can have a direct tradeoff with somatic regeneration[7]. These findings suggest that competing demands can limit the resources that are available for repairing somatic damage, which ultimately leads to damage accumulation and may affect lifespan.

Alternatively, seminal experiments in *C. elegans* have demonstrated that ablating the germline can produce remarkable lifespan extension[8–10], but only when the empty somatic gonad remains intact (i.e. not via full castration). These findings suggest that the longevity phenotype is not just a consequence of a trade-off in resources, but rather depends on endocrine signals mediated by the gonad; either pro-longevity signals released by an empty gonad, or loss of pro-aging signals released from the intact gonad. Downstream, enhanced pro-longevity pathways were detected in germline-ablated worms, including proteostasis and lipid metabolism[11]. Intriguing correlative data exists in humans, as well as several farm and laboratory animals, whereby removal of both the somatic gonad and the germline through castration (e.g. in Korean eunuchs) can have a profound effect on longevity [12–19]. Thus, additional experimental evidence is required to determine how the germline itself can impact vertebrate lifespan, and to elucidate the relative contribution of each of the seemingly opposing theories described above[20–23].

Unlike worms, vertebrate reproduction is regulated by the vertebrate-specific hypothalamic–pituitary–gonadal (HPG) axis. Therefore, paradigms cannot be simply extrapolated from studies in *C. elegans*. In addition, most vertebrates are segregated into true females and males, thereby introducing the possibility of investigating sex-specific effects. Exploring the described concepts in a vertebrate model may therefore provide insights concerning sexual dimorphism in lifespan regulation[24–29]. However, moving away from invertebrates to a vertebrate model introduces new challenges, one of which is the relatively long lifespan of classical vertebrate models that hampers large-scale genetic interrogations. Therefore, the development of alternative experimental strategies is required.

As the most diverse group of vertebrates, fish species exhibit a vast range in life-history[30–33]. For example, the long-lived rockfish and Greenland sharks mature after decades (and even centuries)[34,35]. At the other extreme, the naturally short-lived African turquoise killifish (*Nothobranchius furzeri*) can undergo sexual maturation as fast as 14 days[36], and experience a median lifespan of only ~4-6 months[37–43]. Accordingly, the naturally compressed lifespan of the killifish is 6-10-fold shorter than the lifespan of mice and zebrafish, respectively. Thus, providing a unique opportunity for rapid exploration of vertebrate physiology. The turquoise killifish has vertebrate-

conserved organs and systems, including the HPG reproductive axis, and a recently developed state-of-the-art genome engineering platform[41–49]. However, the regulatory mechanisms of reproduction and gonadal development in killifish are largely unknown.

Most genetic studies of gonadal development in fish have used the zebrafish (*Danio rerio*) and medaka (*Oryzias latipes*) models, but these exhibit unique characteristics. For example, both of these fish depend on the presence of the germline to develop into females (i.e. sterile fish undergo an all-male sex-reversal)[50,51], and zebrafish lack an XY-based sexual determination system[52]. Thus, although recent studies have begun to characterize fish gonads at the single cell level[53], it is currently unknown which patterns are conserved in killifish.

Here, we leverage the turquoise killifish to dissect the link between reproduction and vertebrate lifespan. To this end, we first generate a gonadal cell-type atlas at a single cell resolution, in both male and female fish. This detailed resource allows us to identify primary gonadal cell-types and provide molecular markers for downstream phenotypic analysis. We then generate a panel of genetic models to perturb the reproductive state in killifish, and measure the tradeoff with key physiological properties, including somatic growth and damage repair. Thus, allowing us to dissect the systemic effects of distinct paradigms of germline manipulation in a vertebrate model.

Our results indicate that only depleting the germline, and not blocking germline differentiation, can enhance female-specific somatic repair. To further explore these sex differences, we characterize the liver transcriptome and apply single-cell RNA sequencing for germline-depleted gonads. We reveal a distinct transcriptional response to germline depletion, including an overlap with mammalian pro-longevity interventions. Accordingly, we find that germline depletion can significantly promote longevity in a male-specific manner (~50% increase in maximal lifespan).

To explore evolutionary conservation, we demonstrate that *eef1a1*, a differentially expressed candidate gene, is functionally required for the longevity of germline-depleted *C. elegans*. Finally, we use multi-omics and physiological assays to demonstrate that old germline-depleted males experience prolonged healthspan through enhanced metabolic functions. Taken together, the observed sexual dimorphism supports the notion that classical evolutionary tradeoffs could be uncoupled, and involve a possible systemic effect. Our findings propose that distinct flavors of the reproductive state can have a profound impact on vertebrate life-history.

Results

Reconstruction of the killifish gonadal architecture by single-cell RNA sequencing

As a relatively new vertebrate model, the cell types that constitute the killifish reproductive system and their corresponding molecular markers are largely unknown. Furthermore, determining gonadal composition will be imperative for downstream analysis such as how distinct gonadal cell types respond

to perturbations of the reproductive state. We therefore collected single-cell transcriptomes from one-month-old testis and ovaries to examine the gonadal composition and cell types involved. This age was chosen because killifish have already gone through sexual maturation at this time, and all cell types should be present. Gonads from three male and three female fish were dissociated enzymatically, and single-cell droplet barcoding was performed using the InDrop approach[54–56] (**Figure 1a**). Following quality control, we recovered a total of 5695 single-cell transcriptomes. As the first step, the cells were clustered using uniform manifold approximation and projection (UMAP) and the Leiden algorithm, to distinguish between the germline (gray) and somatic cells (blue) by using conserved germline markers (**Figure 1b**, top left, and **Figure S1a**). Finally, we also performed batch correction by applying the Harmony tool[57] (see **Methods**).

Distinct somatic and germ cell populations in male and female gonads

Vertebrate ovaries and testes are composed of several primary cell types, including supporting, steroidogenic, interstitial, and germ cells. In females, the supporting Granulosa cells are in direct contact with the oocytes, with a layer of steroidogenic Theca cells on top. In males, the supporting Sertoli cells enclose the germ cells, while the steroidogenic Leydig cells are located in clusters spread across the interstitium. To focus on the somatic gonad, we first filtered out the germline (**Figure 1b**, bottom left), grouped the somatic cells into 12 clusters (**Figure 1b**, right), and characterized their cell types based on the expression of conserved markers[53,58–68] (**Figure 1c, d**). A list of all markers associated with each cluster and a list of specific killifish paralogues are available in **Tables S1, S2**.

We then confirmed the spatial architecture of the killifish gonad. Specifically, we selected evolutionary conserved cell-type-specific markers for the somatic compartment[58,61–64] (**Figures 1c, d**), and performed single molecule fluorescent in-situ hybridization chain reaction (smFISH HCR, **Figure 1e**). These markers included *star* (*steroidogenic acute regulatory protein*, for Leydig cells), *amh* (*anti-mullerian hormone*, for Sertoli cells), and the lowly expressed gonadotropin receptor *fshr* (*follicle stimulating hormone receptor* for Granulosa cells). Additionally, we included a germ cell marker as a reference (*ddx4/vasa*, *dead-box helicase 4*[69]).

To better characterize the germline compartment, we performed a sub-clustering analysis for germ cell populations, which included 4294 male sperm cells, and only 74 female oocytes (**Figure S1b**). The difference in capture efficiency can be attributed to the larger size and relative scarcity of female oocytes, which tends to exclude them from our droplet-based pipeline. Similar to the somatic cells, predictions of cell-type specific markers were made based on the expression of conserved markers[58,61–64] (**Figure S1c-d**). A comparison and partial overlap were also seen with similar single-cell experiments, recently performed in zebrafish[53,64] (**Figure S1e**). A possible differentiation trajectory of germ cells is demonstrated through stage-specific germ cell markers[53,58,61,64] (**Figure S1b**), such as *ddx4* (spermatogonia), *dmc1* (*DNA meiotic recombinase 1*, which is expressed in early meiotic germ cells),

and *tekt1 (tektin-1*, which is expressed primarily in differentiated spermatids). One remaining cluster seemed to be of a mixed germline population (**Figure S1b-c**, light green), and another contained residual erythroid cells (**Figure S1b-c**, turquoise).

These results, coupled with smFISH (**Figure S1f, g**), demonstrated that germ cell clusters are largely organized according to a developmental trajectory (**Figure S1b**). The full list of differentially expressed genes of each germline cluster is presented in **Tables S1, S3**. Combining single-cell transcriptomics with smFISH, made it possible to identify somatic- and germline-derived gonadal cell types in killifish. Overlaying the identified marker genes with gonadal histology and teleost gonadal architecture[70–72] allows us to propose a model for the male and female killifish gonads (**Figure 1f**). Thus, providing the foundations for exploring the killifish reproductive state. For example, distinct molecular markers are important to better evaluate cell-type-specific responses to perturbation of the reproductive axis, such as the transcriptional signature or a distinct cell type, or changes in cell composition.

Systematic perturbation of the HPG reproductive axis in killifish

The hypothalamic-pituitary-gonadal axis (HPG) plays a central role in controlling vertebrate puberty. Specifically, the follicle stimulating hormone (FSH) and luteinizing hormone (LH) are released by the pituitary, bind to their gonadal receptors, and support ovary and testis development. In turn, sex steroid hormones are secreted from the gonads, and feed back to the brain to fine tune hormone levels (**Figure 2a**). Although the HPG is largely vertebrate-conserved, there are subtle differences between fish and mammals, which give rise to altered regulatory networks[73,74].

As the first step in manipulating killifish reproduction, we genetically perturbed the HPG reproductive axis by mutating genes that correspond to primary pituitary hormones (FSH and LH), and their corresponding gonadal receptors (FSHR and LHR, respectively). Specifically, using CRISPR/Cas9 genome editing, followed by outcrossing for several generations to reduce off-target effects, we produced the following homozygous mutants: $fshb^{in1/in1}$, $fshr^{in2/in2}$, $lhb^{\Delta 8/\Delta 8}$, and $lhr^{\Delta 10/\Delta 10}$ (**Figure 2b**). Germline maturation was assessed by staining tissue sections with Hematoxylin and Eosin (H&E), and scoring the proportion of specific developmental stages[71,72], in both females (**Figures 2c, d**) and males (**Figure S2a, b**). Our findings demonstrate that, as in zebrafish and medaka[73–78], female germ cell maturation is arrested at distinct stages in response to mutating *fshb*, *lhb*, or their corresponding receptors, and these mutants are therefore largely infertile (**Figure 2e**).

In fish, one of the main energy and metabolic investments during female reproduction is in vitellogenesis[79,80]; the resource-intensive process of yolk formation via nutrient deposition into the oocyte. Our results indicate the $fshb^{in1/in1}$ and $fshr^{in2/in2}$ female mutants display a striking increase in the proportion of previtellogenic eggs (stage PV), at the expense of vitellogenic and mature eggs (stages V and M, respectively, **Figure 2d**). No effect was observed in oocytes during the early developmental

stages of primary growth (stage PG). This observation implies that oocyte maturation is arrested before vitellogenesis. Conversely, female mutants for *lhb* and its receptor *lhr* exhibit an increase in vitellogenic oocytes (stage V), but a decrease in mature oocytes (stage M). Thus, suggesting that oogenesis is arrested at a later stage, before final maturation in these mutants (**Figure 2d**). There is no significant effect on male growth or germline development, and all mutants (aside from male $lhb^{\Delta 8/\Delta 8}$, which is discussed below) were produced at the expected Mendelian ratios (**Figures S2a-e**).

Together, our results reveal developmental windows in which gonadotropins are required for distinct stages of female killifish germline differentiation (summarized in **Figure 2f**). However, even though several theories predict that perturbing reproduction could have a tradeoff with other life-history traits, such as growth, none of the HPG mutants exhibited any significant effect on somatic growth (**Figure S2d**).

Hormonal loss-of-function can be phenotypically rescued

All HPG knockout females are largely infertile (**Figure 2e**). To test whether the phenotypes in $lhb^{\Delta 8/\Delta 8}$ mutants are directly mediated by the loss of hormone function, we attempted to restore fertility experimentally. Specifically, we used a platform for functional interrogation of peptide hormones, which we have recently developed for killifish[49], to ectopically express hormones in muscle tissue (**Figure S2f**, left). These hormones are then predicted to be secreted into the circulation and ultimately reach the gonads. *Lhb* was cloned from turquoise killifish cDNA and tagged with GFP separated by the T2A self-cleaving peptide, which leaves the hormone untagged after cleavage.

This approach allowed us to restore oocyte differentiation and female fertility to $lhb^{\Delta 8/\Delta 8}$ mutants (**Figure S2f**, right). A similar rescue was also described in $fshb^{in1/in1}$ as part of the method development[49]. These results suggest that the observed reproductive phenotypes are indeed directly attributed to a loss of hormone function. Our conclusions are further supported by the undetected transcript levels of the receptor in the corresponding *lhr* and *fshr* homozygous mutants, as evaluated by smFISH (probably due to nonsense-mediated mRNA decay, **Figure S2g**).

Chromosome conformation capture (Hi-C) places *lhb* in proximity to the killifish sex locus

Curiously, although most HPG mutants were produced at the expected Mendelian ratios, $lhb^{\Delta 8/\Delta 8}$ mutant males were rarely observed (**Figure S2c**). This raised the possibility that the gene is located near the killifish sex determination gene *gdf6*[45] (*growth differentiation factor 6*) on chromosome 5, and therefore, is not equally segregated between males and females. Since *lhb* (LOC107396183) is currently on an unplaced genomic scaffold, we performed chromosome conformation capture (Hi-C[81–83]) and used it to scaffold the killifish genome. This indeed demonstrated that the *lhb* gene is located only 11 Mb away from the sex locus (**Figure 2g** and see **Methods** for details). The full description of the Hi-C analysis, including the identification of the topologically associated domains (TADs, the fundamental

units of the 3D nuclear organization), will be reported elsewhere (M.D. and I.H, unpublished data). Additionally, by generating 814,717,494 Hi-C reads, our analysis also corrects many large-scale errors in the killifish genome and assists in positioning short contigs within chromosomes (improving the N90 from 152,787 to 298,000 and reducing scaffold numbers from 5,897 to 2,614, **Figure S2h**).

Germline depletion enhances somatic repair in a sex-specific manner

One prediction of the 'disposable soma theory' is that perturbing reproduction should have a tradeoff with other physiological traits, particularly somatic damage repair[4,6]. To test this, we selected the infertile *fshr*$^{in2/in2}$ and *lhr*$^{\Delta 10/\Delta 10}$ mutants, in which oocyte development is blocked at early stages, either before the resource-intensive vitellogenesis process[79,80] or before oocyte maturation, respectively (**Figure 2 c-d**). The alternative 'endocrine signals' hypothesis suggests that physiological traits will be altered only by completely removing the germline (while the somatic gonad remains intact). Therefore, to simulate this physiological scenario we mutated the *dnd1* gene (*dead end*[84–86]) to produce a germline-depleted killifish model (**Figure 3a**, left).

Dnd1 was previously shown to be essential for germline formation in fish, because it is responsible for regulating primordial germ cell migration into the embryonic somatic gonad[84–86]. Accordingly, *dnd1*$^{\Delta 4/\Delta 4}$ homozygous killifish mutants are germline-free (**Figure 3a**, right). Similar to the HPG mutants described above, *dnd1*$^{\Delta 4/\Delta 4}$ fish displayed no apparent tradeoff with somatic growth (**Figure S3a, b**). Germline depletion in either zebrafish or medaka causes an all-male sex-reversal[50,51], which precludes the study of sexual dimorphism (particularly females). However, both male and female germline-free *dnd1*$^{\Delta 4/\Delta 4}$ killifish were obtained at the overall expected Mendelian ratios (**Figure S3c**). Thus, demonstrating that much like in mammals, killifish undergo germ-cell-independent sex differentiation.

To evaluate the effect of *dnd1*$^{\Delta 4/\Delta 4}$, *fshr*$^{in2/in2}$, and *lhr*$^{\Delta 10/\Delta 10}$ on somatic damage repair, we assessed tail regeneration capacity following irradiation as a proxy for a physiological challenge (as recently tested in zebrafish[7]). Killifish were first exposed to a sub-lethal level of whole-body ionizing radiation (X-ray, 20 Gy), and regenerative potential was assessed by measuring the rate of tail-fin regrowth following amputation (**Figure 3b, c**). Interestingly, while the homozygous *lhr*$^{\Delta 10/\Delta 10}$ and *fshr*$^{in2/in2}$ mutations had no apparent effect, regeneration was significantly enhanced in germline-free *dnd1*$^{\Delta 4/\Delta 4}$ fish, specifically in females (**Figures 3d, S3d**). We did not test HPG mutants in males (**FigureS3d**), as they had no germline phenotype (**Figures S2a, b**). Even though killifish tail regeneration is also inhibited during natural aging[87], the *dnd1*$^{\Delta 4/\Delta 4}$ mutation did not enhance tail regeneration in old fish (**Figure S3e**). We therefore conclude that the benefits of enhanced regeneration in females might only be obtainable in response to a particular stress.

The zebrafish study described above has recently suggested that once the 'expensive' germline is damaged via genotoxic stress, germline repair itself can have a direct tradeoff with somatic

regeneration[7]. These experiments offer an interesting prediction, proposing that irradiating the entire body (both the tail and the germline) would have a different outcome when compared to tail-specific irradiation. To compare these two possibilities, we exposed WT fish to the same dose of radiation, either whole-body or tail-specific irradiation (to avoid damaging the gonad, **Figure S3f**). Even though only whole-body irradiation induced extensive damage to the germline, both interventions equally inhibited tail regeneration (**Figure S3g**). Thus, our data suggest an alternative interpretation to the findings in zebrafish[7]. Specifically, our findings suggest that the resources required to repair the damaged germline might not be the primary reason for the observed phenotypes, but rather the direct damage the tail has sustained.

Finally, we tested whether different flavors of the reproductive state can induce other physiological changes that correlate with the observed phenotypes (**Figure 3d**). Therefore, we examined the histology of the liver, a primary metabolic organ that is involved in the energy production required for vitellogenesis. We characterized the accumulation of hepatocellular vacuolizations[88,89], which are either lipid-type (round, sharp edges) or glycogen-type (irregular, lightly stained) (**Figure S3h**). Our results indicated that overall, there was no strong correlation between the severity of the gonadal phenotype and the metabolic effect. For example, in all female mutants we observed an accumulation of primarily glycogen-type vacuoles (**Figure S3i**). However, similar trends were observed between *lhr* $^{\Delta 10/\Delta 10}$*and dnd1*$^{\Delta 4/\Delta 4}$. Similarly, characterization of internal visceral adipose tissues[90] suggested that both *fshr*$^{in2/in2}$ and *dnd1*$^{\Delta 4/\Delta 4}$ female mutants experience lipid accumulation, while WT and *lhr* $^{\Delta 10/\Delta 10}$ remained lean (**Table S4**).

So far, our results indicate that only specific reproductive defects, namely germline depletion, can enhance somatic maintenance in a sex-specific manner (an 'all or none' effect). This suggests that the observed phenotypes may not be limited to a classical tradeoff, which predicts a more gradual phenotype that inversely correlates with the resources invested in the germline (for a summary, see model in **Figure 3e**). Therefore, to better understand how germline depletion generally affects the surrounding somatic cells, we decided to characterize individual cells, isolated from the empty somatic gonads in *dnd1*$^{\Delta 4/\Delta 4}$ fish.

Single-cell RNA sequencing of germline-depleted gonads in young fish suggests sex-specific physiological responses

A comparison of gene expression profiles in somatic cells, from WT and germline-depleted *dnd1*$^{\Delta 4/\Delta 4}$ gonads, could provide key insight into how germline depletion affects somatic tissue. However, the dominant germline population that is missing in the *dnd1*$^{\Delta 4/\Delta 4}$ mutant gonads precludes the use of bulk RNA sequencing approaches. Therefore, we collected single-cell transcriptomes from one-month-old testis and ovaries of germline-free *dnd1*$^{\Delta 4/\Delta 4}$ fish (**Figures 4a, S4a-c**), to ultimately explore differential gene expression between overlapping cell populations (e.g. WT vs. *dnd1*$^{\Delta 4/\Delta 4}$ fibroblasts).

Germline-depleted gonads are naturally smaller compared to WT (**Figure 3a**, as also seen in similar worm experiments[8]). This required samples to be pooled to provide enough cells, which prevents the use of individual fish as biological replicates (see **Methods**). Following quality control, we recovered an additional 4361 single-cell transcriptomes from the gonads of *dnd1*$^{\Delta 4/\Delta 4}$ mutants (2539 from males, and 1822 from females). Male and female samples were analyzed separately, and UMAP and batch correction were applied as described above. Cells were then grouped into 11 and 18 clusters, in males and females respectively (**Figures 4a, S4a**, and **Tables S1, S5, S6**).

While germline lineages were completely missing in the homozygous *dnd1*$^{\Delta 4/\Delta 4}$ gonads, primary somatic cell types could be assigned according to the markers identified in WT fish (**Figures 1c-d, 4a, S4a-c**), and could be visualized using smFISH (**Figure 4b**). Some qualitative differences in cell composition were observed, such as a significant increase in monocytes in *dnd1*$^{\Delta 4/\Delta 4}$ female gonads, compared to more neutrophils in WT females ($p < 0.0001$, Fisher's exact test. **Figures 4a, S4a**). Other somatic cell types, such as fully differentiated Granulosa and Theca cells, were not detected in the *dnd1*$^{\Delta 4/\Delta 4}$ gonads (**Figures 4a, S4a**). This is either due to relatively small numbers of these particular cell types or because the terminal differentiation of some supporting cells (i.e. pre-Granulosa to Granulosa and Theca) was shown to require interaction with oocytes[91,92]. We further confirmed these findings using smFISH in *dnd1*$^{\Delta 4/\Delta 4}$ mutant females. Specifically, while we were able to detect widespread expression of *amh* (**Figures 4b S4d**, a marker for both pre- and mature Granulosa), we failed to detect *cyp19a1* in the gonad (a marker for mature Granulosa, **Figure S4d**).

To identify molecular pathways that are enriched following germline depletion, we focused on selected clusters that contained cells from both genotypes (**Figures 4a, S4a**). To identify robust signatures that appear in multiple cell types, we first screened each cell type for genes that are differentially expressed between WT and *dnd1*$^{\Delta 4/\Delta 4}$ mutant cells and conducted pathway enrichments using gene ontology (GO, conducted separately for males and females, **Figure 4c**). The analysis was performed on fibroblasts (in both sexes), neutrophils and ovarian epithelium (in females), and Sertoli and smooth muscle cells (in males) (**Figure 4c**). As most differentially expressed genes were upregulated in the mutant cells we decided to focus on upregulated genes for further analysis. For example, in female neutrophils, we identified 20 downregulated and 96 upregulated genes (FDR of 0.1 and $\log2(FC) > 1.5$, **Table S7**).

Our results highlighted a striking sexual dimorphism in the response to germline depletion. For example, the upregulated genes in female mutants appeared to be associated with translation and ribosome biogenesis (**Figure 4c**). Candidate genes include *eef1a1 (eukaryotic translation elongation factor 1 alpha 1*, **Figure S4e**), which was upregulated in females, while in male mutants it was downregulated. Using smFISH, we further confirmed that *eef1a1* was highly expressed in *dnd1*$^{\Delta 4/\Delta 4}$ ovaries compared to testis. As a control, expression levels in the intestinal crypts were comparable (**Figure 4d**). A similar pattern was observed by focusing on ovarian epithelium, marked by *ptgds*

(*prostaglandin D2 synthase*), in WT and *dnd1*$^{\Delta 4/\Delta 4}$ ovaries (**Figure S4f**). These results are in agreement with the role of protein synthesis in regenerative processes, as seen in neuronal regeneration[93–95], stem cell function[96], liver regeneration[97], and in the response to DNA damage[98]. In contrast, the upregulated genes in male mutants appeared to be more related to stress resistance and protein homeostasis, which are linked to classical pro-longevity pathways[99,100].

Comparing the hepatic transcriptional signature of germline-depleted fish, with classical longevity interventions in young mice

Based on the single-cell transcriptional responses, we first set to explore whether a similar pro-longevity signature exists in other peripheral tissues. Therefore, we characterized the hepatic transcriptome of young fish, either WT or germline-depleted (5 weeks old). The differential expression analysis revealed a total of 2031 downregulated and 1665 upregulated genes (FDR of 0.05, **Table S8**).

While many genetic, pharmacological, and dietary interventions can extend murine lifespan, we were curious to explore which classical longevity interventions in mice display a similar transcriptional signature to germline depletion. Therefore, we compared our findings with a recent dataset that characterized the hepatic transcriptional responses to 8 different longevity interventions (in young male and female mice[101], **Figure 5a**). These interventions include rapamycin, caloric restriction (CR, 40%), methionine restriction (MR, 0.12%), growth hormone receptor knock-out (GHRKO), acarbose, 17-α-estradiol (17α-E2), Protandim (a weak Nrf2 activator), and Pit1 knockout (Snell dwarf).

Specifically, we performed functional enrichment analysis for differentially expressed genes in germline-depleted young fish and compared them with enriched pathways in the mouse dataset[101] (**Figure 5a** and **Table S8**). Applying unsupervised clustering assisted us in identifying that germline depletion primarily clustered with 17α-E2, for both males and females (**Figure 5a**). Within this cluster, partial pathway overlaps include activation of ERK signaling, modified immune response, and carbohydrate metabolism. Other pathways were more enriched in one sex compared to the other, such as cellular response to starvation (male killifish), and tissue regeneration (female killifish). Together, our findings provide important insights into possible mechanisms of action that might be shared with other longevity interventions, such as 17α-E2[102–106].

Germline depletion extends male lifespan

So far, the liver and single-cell data prompted further examination of the long-term effects of germline depletion on lifespan. To exclude other possible costs of reproduction, particularly mating and physical damage due to competition[107], animals were single-housed throughout their lives. Excitingly, we observed a male-specific lifespan extension (**Figure 5b**, $p = 0.02$, log-rank test), while the lifespan of female *dnd1*$^{\Delta 4/\Delta 4}$ mutants remained unchanged ($p = 0.69$, log-rank test). The longevity effect in males was not uniform across life, as the median lifespan increased by ~11%, while the maximal lifespan by ~50% (90th percentile[108,109]).

We therefore investigated the shape of the lifespan curve by using a Quantile-Quantile (Q-Q) plot, which visually demonstrates how the two experimental groups deviate from one another (**Figure S5a**, left). In a hypothetical case where control and experimental groups are similar, the plot would be along a straight 45° angle line (as seen in a Q-Q plot of female lifespan, **Figure S5a**, right). This is true in our data only up to ~80th percentile (175 days). We validated this analysis by using Boschloo's test[109] at different percentiles. Specifically, we identified that while there is no significant lifespan difference at the 50th and 75th percentiles (p=0.223 and 0.12, respectively), a significant difference was observed at the 90th percentile (p=0.04). These findings are consistent with the 'neck-and-shoulder' lifespan curve previously observed in germline-depleted worms[8,9,110].

In agreement with our sex-dimorphic longevity phenotype (**Figure 5b**), 17α-E2 treatment in mice extends only male lifespan[102–106]. 17α-E2 is a naturally occurring enantiomer of 17β-estradiol (17β-E2), which appears to be non-feminizing due to minimal activation of classical estrogen receptors[106]. Therefore, we next compared whether other common gonadal/hormonal interventions in male mice[101,111,112] (e.g. castration, estrogen receptor KO, hormone replacement) might overlap with the transcriptional response of germline depletion. Our data indicated that germline depletion clusters both with 17α-E2 treatment, which requires an intact gonad for promoting male longevity[104,113], as well as with castration alone (**Figure S5b**). However, since castration cancels the longevity benefit of 17α-E2 in mice, the physiological effects of 17α-E2 are expected to only partially overlap with castration (**Figure S5b**, right). These partial overlaps provide an important step toward identifying the molecular mechanisms that mediate the longevity benefits of germline depletion.

Our findings demonstrate that germline depletion can enhance longevity and somatic regeneration in a vertebrate model, with no significant tradeoff with somatic growth. The sex-specific phenotypes suggest that the effect is probably mediated by mechanisms other than the classical idea of a tradeoff between primary life-history traits[4,5] - since a missing germline should similarly affect resource allocation in males and females (see a schematic model in **Figure 5c**). Next, we explored evolutionary conservation and possible effects on organismal healthspan.

Exploring evolutionary conservation with germline ablated worms

To investigate evolutionary conservation, we tested whether candidate genes that emerged from our killifish single-cell transcriptomic data can mediate the lifespan extension in germline-depleted worms. We therefore selected the CF1903 strain[9], which harbors a temperature-sensitive mutation in *glp-1* (*e2144*). *Glp-1* is an essential gene for germline maintenance in worms[9]. Accordingly, worm mutants display germline depletion and lifespan extension following a shift to the non-permissive temperature (from 15 to 25°C)[9]. Interestingly, we observed a 'neck-and-shoulder' shape of the survival curve in *glp-1* mutants (**Figure S5c**. representative data from 3 independent lifespan experiments, see **Table S4**). This shape is in agreement with previous findings[9,110], and similar to our killifish data (**Figure 5b**).

We next selected several representative differentially expressed genes as potential modifiers (from **Figure S4e**), and perturbed them using RNAi in the *glp-1* mutants (at the restrictive temperatures). Interestingly, we identified that *eef1a1* is required for the longevity of CF1903 (**Figure S5c**, left). We further confirmed that at the permissive temperature, in the presence of a germline, no lifespan differences were seen between empty vector (EV) and the *eef1a1* RNAi-fed worms (**Figure S5c**, right). This genetic interaction suggests a possible evolutionary-conserved mechanism that mediates the longevity effect of germline depletion. Next, we characterized the physiological effects of germline depletion on male killifish healthspan.

Germline depletion produces a distinct transcriptional response in old male killifish

So far, we have characterized the transcriptome of young fish. To further investigate the effect of germline depletion on the aging process, we also characterized the hepatic transcriptome of old fish, either WT or germline-depleted (25 weeks old, **Figure 6a**). Principle component analysis (PCA) indicated that germline depletion produced widespread transcriptional changes in the liver (**Figure S6a**), with some segregation linked primarily to age (PC1), or to sex and genotype (PC2). The differential expression analysis in old fish revealed a total of 135 downregulated and 295 upregulated genes (FDR of 0.05, **Table S8**).

We next conducted gene set enrichment analysis (GSEA) using gene ontology (GO), combining datasets from both young and old fish. While some enrichments in young fish were similar in males and females, several behaviors displayed a sex-specific pleiotropic pattern. For example, nuclear division is down in young mutants, and up in old mutant males (**Figure 6a**). Our analysis further suggested that old germline-depleted males might experience enhanced metabolic functions, among several other longevity-related pathways (e.g. reduced inflammation, increased protein folding). Representative driver genes displaying sex-specific patterns in old age are also indicated (**Figure 6b**), including *ltbr* (*lymphotoxin beta receptor*, inflammatory response), *mki67* (*marker of proliferation ki-67*, nuclear division), *hspa9* (*heat shock protein family a member 9*, protein folding), *map3k3* (*mitogen-activated protein kinase kinase kinase 3*, p38MAPK cascade), and *esr1* (*estrogen receptor 1*, estrogen signaling). Of note is the expression pattern of *mki67*, a classical proliferation marker, which displays a pleiotropic pattern (**Figure 6b**, top right). We next set out to investigate which of these biological processes might be rejuvenated in old germline-depleted males.

Metabolic plasticity is partially restored in germline-depleted males

Our transcriptional analysis identified several pro-longevity pathways in germline-depleted males, including protein folding (**Figures 4c, 6a**) and metabolic functions (e.g. response to starvation, **Figure 5a**). Therefore, in addition to the irradiation stress described above, we decided to test other stressors. *Dnd1* expression is primarily restricted to the germline (**Figure S6b**, top left). However, as we cannot rule out a function for this gene beyond the germline, as a complementary strategy to genetic germline depletion, we used antisense morpholino injections against *dnd1*[7,84] (see **Methods**). In agreement with

prior fish studies[7,84], injection of *dnd1* morpholino briefly inhibits *dnd1* function. This inhibition occurs specifically during early embryogenesis when the germline migrates into the gonad, and then the expression is restored for the remaining fish lifespan.

Morpholino injections were efficient in depleting the killifish germline (~90% efficiency, see **Methods**), and were able to replicate our sex-specific findings following whole-body irradiation (given natural experimental variation, **Figure S6b**, bottom). This approach complements our genetic approach, suggesting that the physiological effects are likely mediated by the depletion of the germline, and not via other *dnd1* functions. We next tested other stressors, including proteostatic or oxidative stress, which mildly inhibit tissue regeneration[114,115] (**Figure S6c**, chloroquine or paraquat treatments, respectively). However, following pharmacological treatments, the regenerative potential was only modestly improved in germline-depleted males (particularly following proteostatic stress, **Figure S6d**).

As these stressors did not produce a robust effect, we decided to explore other parameters that are predicted by our transcriptomic data, such as cell division (**Figure 6a**). In agreement with the observed transcriptomic pattern, quantification of proliferation using EdU demonstrated that germline depletion increases hepatic proliferation in old age (**Figure S6e**). Another prediction from our RNA sequencing data is that germline depletion alters metabolic function, which naturally declines in old killifish[43]. Furthermore, as the longevity effect of 17α-E2 treatment in male mice also involves enhanced metabolic functions[102–106], we explored several metabolic parameters following germline depletion.

While blood glucose content at metabolic baseline (short-term fasting) was not a good aging marker (**Figure 6c**, in agreement with recent fingings[116]), liver histology revealed that vacuoles, both lipid and glycogen type[117–119], are largely depleted with age (**Figure 6d**). Interestingly, these vacuoles are restored to a 'young-like' composition in old germline-depleted fish (**Figure 6d**). We have recently applied multiomics to demonstrate that rejuvenation of metabolic plasticity in killifish is associated with restoration of a robust fasting response[43]. Therefore, to better assess the impact of germline depletion on the killifish fasting response, we applied metabolomics to livers isolated from WT and germline-depleted males at metabolic baseline (**Figures 6e, f, Table S9**).

Out of a total of 140 unique metabolites, all passed our quality control (see **Methods**). Samples seem to segregate according to experimental conditions (PC1, **Figure 6e**), and differentially abundant metabolites were assigned to primary metabolic pathways (according to BioCyc[189] and MetaboAnalyst[190], see Methods. **Figure 6f**). For example, a reduction in the pentose phosphate pathway (PPP) was observed in old germline-depleted fish, as well as altered nucleoside and nucleotide metabolism (i.e. increased GMP and UMP, **Figure 6f**). The PPP is an integral part of the mammalian fasting response[120–123], and inhibition of the PPP promoted longevity in *C. elegans* by mimicking dietary restriction[124]. These trends partially overlap with our recent characterization of a youthful fasting response in killifish[43].

Collectively, the transcriptomic, metabolomic, and histological data suggest that beyond the observed longevity phenotype, germline-depletion might also enhance male healthspan (such as

metabolic functions). Ultimately, identifying the signals involved in mediating this phenotype could provide an exciting opportunity to uncouple the evolutionary link between reproduction and vertebrate lifespan.

Discussion

A tradeoff between life-history traits is traditionally associated with reproduction, repair of somatic damage, growth, and lifespan[125–127]. However, the evidence that some of these tradeoffs can be experimentally uncoupled in invertebrate models, suggests the existence of alternative mechanisms for regulating life-history[128,129]. For example, following germline depletion in worms, the reproductive system can have a direct effect on hermaphrodite longevity via endocrine signals[8,9]. In contrast, complete removal of the gonad (both the germline and the somatic gonad), has no effect in worms. Nonetheless, the direct effect of specific germline manipulations on vertebrate life-history, particularly lifespan, has not yet been thoroughly evaluated[20,21,107,130].

Here, we genetically perturb reproduction by manipulating the germline at discrete developmental stages. Our data suggest that as an alternative to the classic view that any perturbation of reproduction can free up resources for somatic functions[125], different forms of infertility produce different effects on life-history. Thus, the paradigms identified in worms might be conserved in a vertebrate model. It is worth mentioning that the observed longevity phenotypes in worms might be context-dependent. For instance, under favorable environmental conditions (e.g. moderate temperatures), the germline might not have a negative effect on killifish lifespan[131], and therefore might contribute to temperature-dependent variations in longevity[132]. Beyond lifespan, other downstream pathways are enhanced in the soma of germline-ablated worms, including proteostasis and energy/lipid metabolism[11]. Our data suggests that metabolic functions might be rejuvenated (**Figure 6d-f**), and an additional mild effect was detected on proteostasis (**Figure S6c-d**).

Chen et al.[7] have recently proposed a trade-off between somatic and germline repair, which supports the 'expensive germline' hypothesis. Specifically, they have demonstrated that germline-depleted zebrafish can better regenerate their tail following irradiation. However, our data suggests that the regenerative potential of the tail could be independent of whether the germline is damaged or not (**Figure S3f, g**). Additionally, the sex-specific phenotypes seen in killifish following germline depletion further support the concept that some mechanisms might not depend on a classical tradeoff. However, it should be noted that regeneration of WT fish following irradiation was itself sex-dimorphic (**Figures 3d, S3d**). This could suggest that male fish might innately possess enhanced regenerative potential, as the tail plays an important role in mate recognition[133]. Additionally, the differences in regenerative potential between zebrafish and killifish might be attributed to innate physiological differences, such as the all-male sex reversal observed in germline-depleted zebrafish[7].

What can mediate the observed sexual dimorphism? Plausible candidates are the sex-dimorphic circulating hormones[134–137] (**Figure 2a**). Notably, both pituitary and sex hormones have previously been linked to vertebrate longevity, such as growth hormone[138–140] or its receptor[141] . However, as germline-depleted fish were of normal size (**Figure S3a**), other circulating factors might be involved. In humans, exceptional longevity was recently shown to be correlated with the preservation of the integrity of the HPG axis[142]. Modified levels of steroid hormones have also been reported to be linked to longevity[143], regeneration[144,145], metabolism[146–148], and immune functions (e.g. testosterone is an immunosuppressant[80,149,150]). Yet, it is worth mentioning that the pursuit to identify systemic regulators in germline-ablated worms has been ongoing for decades[8,9,20–23].

Gonadal development, particularly gonadal size, depends on the presence of the germline in many species, from humans to worms[8,151]. Accordingly, following germline depletion, the gonad is affected and becomes hypoplastic, which could contribute to the observed phenotypes. Importantly, an "empty" vertebrate gonad can still retain a partial signaling ability[16,50,152–156]. To further investigate this, we applied several strategies. First, by comparing the hepatic transcriptional signature in germline-depleted fish to common longevity interventions in mice, we identify an overlap with 17αE2 treatment, which is thought to be naturally synthesized outside the gonad[157]. Similar to 17αE2-treated mice, germline-depleted killifish males display rejuvenated metabolic functions and reduced 'inflammaging' (**Figures 5, 6**). Along these same lines, the longevity effect of 17αE2 in mice is male-specific and depends on the presence of a gonad[102,113,158].

Further comparison with gonadal/hormonal interventions in male mice (e.g. castration, estrogen receptor KO, hormone replacement) indicated that germline depletion still clusters with 17α-E2 treatment and castration (**Figure S5b**). Interestingly, our recent longevity intervention in killifish, through indirect activation of AMPK, was also male-specific and showed a similar signature to 17αE2 (which involved AMPK activation[106]). These data raise the possibility that part of the effect of germline depletion on lifespan is related to the AMPK pathway. Beyond killifish, our data suggests other possible mediators, such as the involvement of protein translation as a longevity modifier of germline-depleted worms (i.e. *eef1a1*, **Figure S5c**). These partial overlaps are an important step towards identifying downstream mechanisms, and support a possible involvement of the remaining somatic gonad.

The timing of germline depletion might be important in mediating the physiological effect. For example, while early germline depletion in *Drosophila* shortened the female lifespan (with a modest extension of the male lifespan)[159], exclusive elimination of germ cells in late development extended the lifespan of both sexes[160]. The intriguing correlative data in humans and several other farm and laboratory animals demonstrated that removing the entire gonad (e.g. Korean eunuchs, sheep castration) can have profound longevity effects in males (with complex phenotypes following females ovariectomy[12–19]) However, the timing differs from the outcome in *Drosophila*, as men castrated before sexual maturation lived longer than if the castration occurred after sexual maturity[12]. Therefore, it will

be important to develop genetic tools to directly compare castration and germline depletion or to induce germline depletion at specific time points to better compare other possible tradeoffs (e.g. germline stem-cell maintenance).

Finally, germline depletion in killifish primarily affects maximal lifespan (**Figure 5b**). Thus, suggesting another type of 'temporal window' in which longevity benefits are provided primarily during late-life stages. Interestingly, a similar 'neck-and-shoulder' shape of the survival curve was also observed in worms following germline manipulation using different flavors of the *glp-1* mutation[9,110]. These findings are in contrast to effects on median lifespan produced by metabolic interventions in both worms (e.g. *eat-2* mutants[110]) and killifish (i.e. *aprt* mutants[161]). In conclusion, the means by which the germline manipulates organismal physiology could explain how the ratio between age at maturity and organismal lifespan is evolutionarily conserved across so many vertebrate species.

Figure legends:

Figure 1: Reconstruction of somatic cell types in the gonads of the turquoise killifish

(**a**) Experimental workflow for characterizing male and female killifish gonadal cell types using InDrop single-cell RNA sequencing.

(**b**) UMAP analysis of 5695 single cells from the testis and ovary of one-month-old fish. Clusters are color-coded either by somatic- and germ-cells (top left), by somatic cells from males and females (bottom left), or by somatic cell types (right).

(**c**) Dot-plot representing the relative expression of select cell-type marker genes in each cluster. Clusters are color-coded according to (**b**, right). Some markers are shared between cell types, such as cells with similar functions (e.g. *amh* in the supporting Sertoli and Granulosa cells). A full list of cell-type markers can be found in Supplementary **Table S2**.

(**d**) Gene expression UMAP plots of selected marker genes that correlate with primary cell types.

(**e**) smFISH in ovaries (left) and testes (right) for selected markers. Marker for immature germ-cells (*ddx4*) in red (UMAP in **Figure S1d**), and for somatic cell types *(fshr, star, lhr,* and *amh)* in green. Asterix highlights mature germ cells, which are *ddx4* negative. Green arrowheads highlight expression patterns. Representative of $n \geq 6$ individuals. Scale bar: 50 µm for ovary, and 25 µm for testis.

(**f**) A predicted model illustrating the spatial distribution of primary gonadal cell types in killifish ovary and testis, and their associated marker genes. Shapes of sperm cells indicate different developmental stages, from early stages (right) to fully differentiated sperm (left). See detailed differentiation trajectory in **Figure S1f**

Figure S1: Reconstruction of germ cell markers in the gonads of the turquoise killifish

(**a**) Gene expression UMAP plot of a marker gene that correlate with germ cells.

(**b**) Sub-clustering of the germ cells, color-coded by sex (left) or clustered according to Leiden and sex (right). Proposed differentiation trajectory is marked with an arrow.

(**c**) Dot-plot representing the relative expression of select cell-type specific marker genes in each cluster. Clusters are color-coded according to (**b**, right). A full list of all markers can be found in Supplementary **Table S3**.

(**d**) Gene expression UMAP plots of select marker genes that correlate with primary germ cell differentiation states.

(**e)** Dot-plot representing key marker genes of gonadal cell-types identified in zebrafish[53,64], and their relative expression in the corresponding clusters in killifish gonads, either germ cells (left) or somatic cells (right). Clusters are color-coded according to (**b**, right) for germ cells and **Figure 1b** for somatic cells.

(**f-g**) A model of germ cell development in killifish (top), in either males (f) or females (g) (modified from[28]). Bottom: smFISH for selected markers in testis (f) or ovary (g), including markers for supporting cells (*amh*, in red), and for stage-dependent germ cell markers (*ddx4*, *dmc1*, *tekt1*, and *zp4*, in green). Representative of $n \geq 6$ individuals. Scale bar: 25 µm (f) and 50 µm (g). SG: spermatogonia; SC: spermatocytes; ST: spermatids; SZ: spermatozoa; PG: primary growth; PV: pre-vitellogenic; V: vitellogenic; M: Mature.

Figure 2: Genetic perturbation of the reproductive axis in killifish

(**a**) Schematic illustration of the vertebrate hypothalamic-pituitary-gonadal axis (HPG): *fsh* and *lh* are released from the pituitary, and travel through the bloodstream to their target receptors in the gonad to stimulate germ cells production. Top right: an immunostaining for *lhb* (green) and DNA (blue) in histological section of the pituitary in the turquoise killifish. Representative of n =3 individuals. Scale bar: 50 µm.

(**b**) Generation of HPG CRISPR mutants, depicting the guide RNA (gRNA) targets (red), protospacer adjacent motif (PAM, in bold), and indels.

(**c**) Representative histological sections, depicting ovaries from one-month-old females of the indicated genotypes. n ≥ 5 individuals from each genotype. Scale bar: 250 µm. Oocyte development stages: PG: primary growth; PV: pre-vitellogenic; V: vitellogenic; M: Mature.

(**d**) Quantification of oocyte maturation in each of the genotypes from (**c**). Data presented as proportion of each oocyte developmental stage. n ≥ 5 individuals for each experimental group. Significance was measured by χ^2 test with the WT proportion as the expected model and FDR correction. P-values are indicated. Abbreviations represent the oocyte developmental stage according to[102].

(**e**) Quantification of female fertility output. Each dot represents the number of eggs per breeding pair of the indicated genotypes, per week of egg collection. A total of 6 independent pairs and 4 independent collections were performed. Error bars show mean ± SEM with individual points. Significance was calculated using one-way ANOVA with a Dunnet post-hoc compared to the WT and p-values are indicated.

(**f**) A model for the role of gonadotropin signaling in controlling germ cell development in killifish females (modified from[28]). *Fshb* controls follicle growth and the transition from pre-vitellogenic (PV) to vitellogeinc (V), while *lhb* is important for oocyte maturation (M). The specific mutation inhibits the relevant processes.

(**g**) Experimental workflow for Hi-C (left). A genome-wide contact matrix (center), demonstrating the 19 linkage groups (pseudochromosomes) that correspond to the 19 killifish chromosomes. The submatrix (right) corresponds to interactions on pseudochromosome 9 (chromosome 5). Intensity (in red) corresponds to the number of reads/interactions, and tick marks appear every 5 Mb. Locations of the *lhb* gene and the sex determining locus (*gdf6a*) are indicated (red arrows).

Figure S2: Perturbation and rescue of the reproductive axis in killifish

(**a**) Representative histological sections depicting testis from one-month-old males of the indicated genotypes. n ≥ 4 individuals from each genotype (except for *lhb*, which was sex-linked, n=1). Scale bar: 50 µm. Sperm developmental stages according to[102]: SG: spermatogonia; SC: spermatocytes; ST: spermatids; SZ: spermatozoa.

(**b**) Quantification of sperm maturation, examples in (**a**). Data presented as proportion of each developmental stage for each of the indicated genotypes. n ≥ 4 individuals for each experimental group (except for *lhb*, which was sex-linked, n=1). Significance was measured by χ^2 test with the WT proportion as the expected model. P-values are indicated.

(**c**) Distribution of genotype progeny from heterozygous pairs of the indicated genotype (stratified by sex). n = 30-130 individuals, per genotype/sex. Significance was measured by χ^2 test with Mendelian proportions (25:50:25) as the expected model and FDR correction. P-values are indicated.

(**d**) Quantification of somatic growth by calculating the standard length of one-month-old males (left) and females (right) of the indicated genotypes. n ≥ 8 individuals from each genotype. Error bars indicate mean ± SEM with individual points. Significance was calculated using one-way ANOVA and p-values are indicated.

(**e**) Quantification of male fertility. Each dot represents the number of eggs per breeding pair of the indicated genotypes, per week of egg collection (except for *lhb*, which was sex-linked). A total of at least 4 independent pairs and 4 independent collections were performed. Error bars indicate mean ± SEM with individual points. Significance was calculated using one-way ANOVA and p-value is indicated.

(**f**) Schematic illustration for intramuscular ectopic plasmid electroporation (left). GFP is visible following the electroporation of *lhb*-T2A-GFP. Quantification of fertility output (right) in $lhb^{\Delta 8/\Delta 8}$ mutant females following electroporation of *lhb-T2A-GFP*. Each dot represents the number of eggs per breeding pair per week of egg collection. A total of at least 3 independent pairs and 4 consecutive weekly collections were performed. Error bars show mean ± SEM with individual points. Significance was calculated using a two-sided Student's t-test and p-value is indicated.

(**g**) smFISH in the ovaries of the indicated genetic models. Marker for immature germ-cells (*ddx4*) in red, and for *fshr* and *lhr* in green. Representative of n ≥ 6 individuals. Scale bar: 50 µm.

(**h**) Oxford Grid plots (left) showing correspondence between the Hi-C linkage groups (Y axis) and previously predicted chromosomes (X axis) in the turquoise killifish. Positive strand matches are shown in blue, and negative strand matches are shown in red. Cumulative fraction of genes (right) located on Hi-C pseudochromosomes and on contigs in the original assembly (gray). Pseudochromosomes/contigs were ranked by size, the number of annotated genes in each was counted (annotation was transferred using GMAP to map transcripts to the new assembly), and the cumulative fraction was calculated. In the Hi-C scaffolded assembly (black), most small contigs containing genes are placed into the 19 main pseudochromosomes.

Figure 3: Germline depletion enhances somatic regeneration in females

(**a**) Top left: generation of a CRISPR mutant for the *dnd1* gene, depicting the gRNA target (red), PAM (in bold), and indel. Bottom left: images of female gonads from one-month-old fish, either WT or *dnd1*$^{\Delta 4/\Delta 4}$ mutants. Scale bar: 1 mm for WT fish, 0.1 mm for *dnd1*$^{\Delta 4/\Delta 4}$ mutant fish. Right: histological sections of male and female gonads from one-month old fish, either WT or *dnd1*$^{\Delta 4/\Delta 4}$ mutants. Representative of $n \geq 4$ individuals from each genotype. Scale bar: 50 μm.

(**b**) Experimental workflow for assessing tail-fin regeneration following irradiation. Tail fish amputation was performed three days after irradiation, and regrowth was measured every three days for a total of 18 days.

(**c**) Examples of regenerated tails at day 18 post amputation, in male (left pair) or female (right pair), under either control (left of each pair) or irradiated (right of each pair) conditions. The black dashed line represents the amputation plane. Scale bar: 2 mm.

(**d**) Tail-fin regeneration following whole-body irradiation in females. Genotypes and treatments are indicated ($n \geq 12$ per experimental group). The length of the outgrowth was calculated as the percentage of the original fin size (before the amputation). Error bars indicate mean ± SEM. Significance was calculated using repeated-measures two-way ANOVA with a Dunnet post-hoc compared to the irradiated WT, and p-values are indicated.

(**e**) A model summarizing the effect of our genetic perturbations on regenerative potential following irradiation. While a gradual effect is observed on germline differentiation, an “all or none” effect is seen in regeneration potential.

Figure S3: Physiological characterization germline-depleted fish

(**a**) Quantification of somatic growth (standard length) of WT or *dnd1*$^{\Delta 4/\Delta 4}$ one-month-old mutants: males (top) and females (bottom), n ≥ 8 individuals from each genotype. Error bars show mean ± SEM. Significance was measured using a two-sided Student's t-test.

(**b**) Representative images of adult (2.5-month-old) males (top) and females (bottom) WT or *dnd1*$^{\Delta 4/\Delta 4}$ mutant fish. Black arrowheads highlight the presence of eggs in the female representative of n ≥4 individuals. WT fish. Scale bar: 3.5 mm.

(**c**) Distribution of genotype progeny from *dnd1*$^{\Delta 4/+}$ heterozygous pairs (stratified by sex). Significance was measured by χ^2 test with Mendelian proportions (25:50:25) as the expected model and FDR correction. n ≥ 500 fish for each group and p-values are indicated.

(**d**) Tail-fin regeneration following whole-body irradiation in males. Genotypes and treatments are indicated (n ≥ 4 per experimental group). The length of the outgrowth was calculated as the percentage of the original fin size (before the amputation). Error bars indicate mean ± SEM. Significance was calculated using repeated-measures two-way ANOVA with a Dunnet post-hoc compared to the irradiated WT, and p-values are indicated.

(**e**) Tail-fin regeneration during aging, in males (left) and females (right). Fish sex, genotypes, and age are indicated (n ≥ 5 per experimental group). Error bars indicate mean ± SEM. Significance was calculated using repeated measures two-way ANOVA with a Tukey post-hoc, and p-values of the comparison between young and old fish of each genotype are indicated by color-coding.

(**f**) Representative images of apoptosis detected by the TUNEL assay (green) and DNA (PI, in red). Assay was performed in tissue sections of ovaries (top) or testis (bottom), under either control conditions (left), following whole-body irradiation (center) or tail-specific irradiation (right). n≥ 6 individuals in each experimental group. Scale bar: 160 µm.

(**g**) Tail-fin regeneration following whole-body or tail-specific irradiation in males (left) and females (right). Treatments are indicated (n ≥ 11 fish for females and n ≥ 20 for males, for each experimental group). Error bars indicate mean ± SEM. Significance was calculated using repeated-measures two-way ANOVA with a Tukey post-hoc, and p-values are indicated. The significance of each experimental group is color-coded and relates to the comparison to the non-irradiated fish.

(**h**) Representative histological sections depicting livers (left) and adipose tissue (right) from one-month-old fish with the indicated vacuole composition or adiposity. Scale bar: 20 µm

(**i**) Quantification of liver vacuole composition, according to (**h**), in male (left) and female (right) fish of the indicated genotypes. Data presented as proportion of each vacuole-type. 3 histological sections from n ≥ 5 individuals for each experimental group. Significance was measured by χ^2 test with FDR correction, with the WT proportion as the expected model. P-values are indicated.

Figure 4: Single-cell RNA sequencing reveals a sex-specific somatic response to germline depletion

(**a**) UMAP analysis of males (left) and females (right). Clusters are color-coded by cell types. Cell-type markers are listed in Supplementary **Tables S1, S5, S6**. Corresponding color-coded UMAP plots by sex are presented in **Figure S4a**.

(**b**) smFISH in ovaries and testes (as indicated by sex symbols) for selected markers in *dnd1*$^{\Delta 4/\Delta 4}$ mutants. Markers for fibroblasts (*col1a1*) in red, and for other somatic cell type markers (*fshr*, *star*, *amh*, and *ptgds*) in green (as described in **Figure 1e**). Green arrowheads highlight expression patterns. Representative of n ≥ 6 individuals. Scale bar: 25 µm.

(**c**) Enrichment analysis (GO) for upregulated genes in *dnd1*$^{\Delta 4/\Delta 4}$ mutants at the indicated clusters/cell types. Distinct patterns between males and females are observed. GO enrichment was called at FDR < 5%.

(**d**) smFISH for selected markers in gut, including the intestinal crypts and villi as controls (top, and small insets), ovaries (center), and testes (bottom) in *dnd1*$^{\Delta 4/\Delta 4}$ mutants. A marker for translation initiation (*eef1a1*) in green, and for heat shock response (*hspa1a1*) in red. Green and red arrowheads highlight expression patterns. White arrowhead indicates lack of expression. Small insets highlight the intestinal crypts, as controls. Representative of n ≥ 10 individuals. Scale bar: 25 µm.

Figure S4: Characterization of cell type markers and differential gene expression in *dnd1*$^{\Delta 4/\Delta 4}$ mutant gonads

(**a**) UMAP of males (top) and females (bottom), from **Figure 4a**, color-coded by genotype.

(**b-c**) Dot-plot (top left, b, left, c) and UMAPs presenting the expression of select marker genes for males (b) and females (c). Dot-plot clusters are color-coded according to **Figure 4a** (for males and females separately). Note that most of the markers overlap with **Figure 1c**. A full list of markers can be found in Supplementary **Tables S5, S6.**

(**d**) smFISH in ovaries for selected markers in *dnd1*$^{\Delta 4/\Delta 4}$ mutants. *Amh* (red), a marker for Pre- and mature Granulosa cells, and *cyp19a1* (green), a specific marker for mature Granulosa. Note that *cyp19a1* is expressed in the adjacent adipose tissue. Representative of $n \geq 4$ individuals. Scale bar: 20 µm.

(**e**) Log2 fold-change heatmap represents the gene expression ratio between WT and *dnd1*$^{\Delta 4/\Delta 4}$ fish of the indicated cell-types. The genes were selected as they were similarly altered in several cell types.

(**f**) smFISH in WT fish and *dnd1*$^{\Delta 4/\Delta 4}$ ovaries. *eef1a1*, a marker for translation initiation (green), and *ptgds*, a marker for ovarian epithelium (in red). Representative of $n \geq 4$ individuals. Scale bar: 20 µm.

Figure 5: Germline depletion extends male lifespan

(**a**) Heatmap for normalized enrichment scores (NESs) in the liver, comparing the response to lifespan-extending interventions in mice with young *dnd1*$^{\Delta 4/\Delta 4}$ mutant fish (left, selected pathways highlighted on the right) A full list of pathways can be found in Supplementary **Table S8**.

(**b**) Lifespan of WT and *dnd1*$^{\Delta 4/\Delta 4}$ fish, assessed separately for males (left) and females (right). P-values for differential survival in log-rank tests, maximal lifespan (measured at the 90th percentile), and fish numbers are indicated.

(**c**) A schematic model proposing that germline depletion (top) can regulate somatic regeneration (upper center) and longevity (lower center) in a sex-specific manner, with no significant tradeoff with somatic growth (bottom).

Figure S5: Germline depletion extends male maximal lifespan

(**a**) Quantile-Quantile (Q-Q) plots for the survival data of WT and *dnd1*$^{\Delta 4/\Delta 4}$ fish (shown in **Figure 5b**), assessed separately for males (left) and females (right).

(**b**) Heatmap for normalized enrichment scores (NESs) in the male liver, comparing the response to gonadal and hormonal treatments in mice with germline-depleted young fish (left, selected pathways highlighted on the right). A full list of pathways can be found in Supplementary **Table S8**.

(**c**) Lifespan of *C. elegans* from *glp-1*(e2144) mutant, grown either at 25°C (restrictive, no germline) or 15°C (permissive, with germline), and fed with the indicated RNAi. Initial mini-screen (left), and confirmation for *eef1a* (right). P-values were calculated according to log-rank with an FDR correction, comparing all experimental conditions to baseline (germline-depleted worms fed with an empty vector at 25°C). Worm numbers for each group can be found in **Table S4**.

Figure 6: Germline depletion rejuvenates male hepatic metabolism

(**a**) Dot plot for functional enrichments (GO, FDR < 5%) using GSEA for differential gene expression between WT and *dnd1*$^{\Delta 4/\Delta 4}$ mutant fish. Sex and age are indicated.

(**b**) Relative expression (normalized to male WT) of driver genes from the pathways in (**a**). Error bars show mean ± SEM with individual points from n ≥ 4 individuals. Significance was calculated as part of the edgeR pipeline in differential expression analysis between WT and *dnd1*$^{\Delta 4/\Delta 4}$ mutant fish.

(**c**) Blood glucose levels of the indicated experimental groups at metabolic baseline. n ≥ 5 individuals in each experimental group. Error bars indicate mean ± SEM. Significance was calculated using one-way ANOVA and exact p-value is indicated.

(**d**) Quantification of liver vacuole composition in male fish of the indicated experimental condition at metabolic baseline (according to **Figure S3h**). Data presented as proportion of each vacuole-type. n ≥ 5 individuals for each experimental group. Significance was measured by χ^2 test with the young WT proportion as the expected model and FDR correction. P-values are indicated.

(**e**) PCA for hepatic metabolite levels of WT (red) or *dnd1*^{morphant} (blue) old male fish. n ≥ 5 samples per condition. Each symbol represents an individual fish.

(**f**) Heatmap showing metabolites that display a significantly altered response between old WT and germline-depleted male fish at metabolic baseline, significance was calculated using a two- sided Student's t-test (p<0.05). Each square represents normalized relative abundance, from an average of n ≥ 5 fish.

Figure S6: Germline depletion enhances regeneration under several stressors

(**a**) PCA for hepatic transcript levels. Groups include male (blue) or female (red), WT (dark shades) or *dnd1*$^{\Delta 4/\Delta 4}$ (light shades), either young (circles) or old (triangles). n ≥ 3 samples per condition, and each symbol represents an individual fish.

(**b**) Top, left: gene expression UMAP plot of *dnd1* gene. Right and bottom: tail-fin regeneration of WT and *dnd1*^{morphant} fish following whole-body irradiation. n ≥ 4 individuals for males, n ≥ 7 for females. Error bars indicate mean ± SEM. Significance was calculated using repeated-measures two-way ANOVA with a Dunnet post-hoc, compared to WT irradiated fish, and p-values are indicated.

(**c**) Tail-fin regeneration of WT fish following treatment by chloroquine or paraquat. Treatments and sexes are indicated. n ≥ 5 fish for each experimental group. Error bars indicate mean ± SEM. Significance was calculated using repeated-measures two-way ANOVA with a Sidak post-hoc, and p-values are indicated.

(**d**) Tail-fin regeneration of WT and *dnd1*^{morphant} fish following treatment by chloroquine or paraquat. Treatments and sexes are indicated. n ≥ 5 fish for each experimental group. Error bars indicate mean ± SEM. Significance was calculated using repeated-measures two-way ANOVA with a Sidak post-hoc, and p-values are indicated.

(**e**) Right: Representative images of proliferation detected in the livers of male fish of the indicated experimental groups, following a 3-day treatment of EdU (green, see **methods**) with DAPI (blue) for detecting nuclei. Representative of n ≥ 5 individuals per group. Scale bar: 50 μm. Left: Quantification of the percentage of proliferating cells. Error bars indicate mean ± SEM. Significance was calculated using one-way ANOVA with a Tukey post-hoc, and p-values are indicated.

Acknowledgements

We thank Alon Zaslaver, Eran Meshorer, Anne Brunet, Yonanan Tzur, Mor Nitzan, and the Harel lab for stimulating discussion and feedback on the manuscript. We thank Ariel Velan, Ella Yanay, Ashayma Abu-tair, Yonatan Birenbaum, Fatma Idrees and Reem Barakat for help with killifish maintenance, Naomi Melamed-Book from the imaging facility (HUJI) and Sergey Malitsky and Maxim Itkin from the Life Sciences Core Facilities, Metabolic Profiling Unit (WIS). Supported by ERC StG #101078188 (IH), the Zuckerman Program (I.H.), Abisch-Frenkel Foundation 19/HU04 (I.H.), ISF 2178/19 (I.H.), Israeli Ministry of Science 3-17631 (I.H.), 3-16872 (I.H.), the Moore Foundation GBMF9341 (I.H.), BSF-NSF 2020611 (I.H.), the Israeli Ministry of Agriculture 12-16-0010 (I.H), the Levi Eshkol scholarship of the Israeli Ministry of Science (E.M.), the Czech Science Foundation (#22-01781O), and the Ministry of Education, Youth and Sports of the Czech Republic (#CZ.02.1.01/0.0/0.0/16_025/0007370) (RF), the Chan Zuckerberg Initiative 2017-174468 and 2018-182817 (W.J.G.), and NIH grant numbers P50HG007735, UM1HG009442, 1UM1HG009436 (W.J.G.).

Author Contributions

E.M., T.A., and I.H. designed the study. E.M. and R.F. performed experiments, E.M. generated the HPG and *dnd1* mutant killifish lines. X.S. and E.M. prepared the single-cell RNA libraries under the supervision of O.R. and I.H., respectively. T.A. designed and performed the analysis of single-cell RNA sequencing under the supervision of I.H.. A.S. performed worm lifespan experiments under the supervision of E.C.. T. A. and E. M. performed statistical analyses, with help from S.S. and D.M.Z.. A.O.G, G.K.M. and W.J.G. performed and analyzed the Hi-C data. T.A., E.M., and I.H. wrote the manuscript. All authors commented on the manuscript.

Ethics declaration

The authors declare no competing interests.

References:

1. Ricklefs, R. E. Life-history connections to rates of aging in terrestrial vertebrates. *Proc. Natl. Acad. Sci.* (2010) doi:10.1073/pnas.1005862107.

2. de Magalhães, J. P., Costa, J. & Church, G. M. An analysis of the relationship between metabolism, developmental schedules, and longevity using phylogenetic independent contrasts. *J Gerontol A Biol Sci Med Sci* **62**, 149–160 (2007).

3. Austad, S. N. & Hoffman, J. M. Is antagonistic pleiotropy ubiquitous in aging biology? *Evol. Med. public Heal.* **2018**, 287–294 (2018).

4. Kirkwood, T. B. L. & Austad, S. N. Why do we age? *Nature* **408**, 233–238 (2000).

5. Kirkwood, T. B. L. Evolution of ageing. *Nature* **270**, 301–304 (1977).

6. Schumacher, B., Garinis, G. A. & Hoeijmakers, J. H. J. Age to survive: DNA damage and aging. *Trends Genet.* **24**, 77–85 (2008).

7. Chen, H. Y., Jolly, C., Bublys, K., Marcu, D. & Immler, S. Trade-off between somatic and germline repair in a vertebrate supports the expensive germ line hypothesis. *Proc. Natl. Acad. Sci. U. S. A.* (2020) doi:10.1073/pnas.1918205117.

8. Hsin, H. & Kenyon, C. Signals from the reproductive system regulate the lifespan of C. elegans. *Nature* **399**, 362–366 (1999).

9. Arantes-Oliveira, N., Apfeld, J., Dillin, A. & Kenyon, C. Regulation of life-span by germ-line stem cells in Caenorhabditis elegans. *Science (80-.).* **295**, 502–505 (2002).

10. Volovik, Y., Marques, F. C. & Cohen, E. The nematode Caenorhabditis elegans: a versatile model for the study of proteotoxicity and aging. *Methods* **68**, 458–464 (2014).

11. Khodakarami, A., Saez, I., Mels, J. & Vilchez, D. Mediation of organismal aging and somatic proteostasis by the germline. *Front. Mol. Biosci.* **2**, 3 (2015).

12. Hamilton, J. B. & Mestler, G. E. Mortality and survival: comparison of eunuchs with intact men and women in a mentally retarded population. *J. Gerontol.* (1969) doi:10.1093/geronj/24.4.395.

13. Min, K. J., Lee, C. K. & Park, H. N. The lifespan of Korean eunuchs. *Curr Biol* **22**, R792-3 (2012).

14. Benedusi, V. *et al.* Ovariectomy shortens the life span of female mice. *Oncotarget* **6**, 10801 (2015).

15. Asdell, S. A., Doornenbal, H., Joshi, S. R. & Sperling, G. A. The effects of sex steroid hormones upon longevity in rats. *Reproduction* **14**, 113–120 (1967).

16. Cargill, S. L., Carey, J. R., Müller, H. G. & Anderson, G. Age of ovary determines remaining life expectancy in old ovariectomized mice. *Aging Cell* **2**, 185–190 (2003).

17. Hoffman, J. M., Creevy, K. E. & Promislow, D. E. L. Reproductive capability is associated with lifespan and cause of death in companion dogs. *PLoS One* **8**, e61082 (2013).

18. Hamilton, J. B. Relationship of castration, spaying, and sex to survival and duration of life in domestic cats. *J. Gerontol.* **20**, 96–104 (1965).

19. Torre, S. Della, Benedusi, V., Fontana, R. & Maggi, A. Energy metabolism and fertility—a balance preserved for female health. *Nat. Rev. Endocrinol.* **10**, 13–23 (2014).

20. Antebi, A. Regulation of longevity by the reproductive system. *Exp Gerontol* **48**, 596–602 (2013).

21. Uno, M. & Nishida, E. Lifespan-regulating genes in C. elegans. *NPJ aging Mech. Dis.* **2**, 1–8 (2016).

22. Ermolaeva, M. A. *et al.* DNA damage in germ cells induces an innate immune response that triggers systemic stress resistance. *Nature* **501**, 416–420 (2013).

23. Calculli, G. *et al.* Systemic regulation of mitochondria by germline proteostasis prevents protein aggregation in the soma of C. elegans. *Sci. Adv.* **7**, eabg3012 (2021).

24. Mauvais-Jarvis, F. Sex differences in metabolic homeostasis, diabetes, and obesity. *Biol. Sex Differ.* **6**, 1–9 (2015).

25. Austad, S. N. Sex differences in longevity and aging. *Handb. Biol. Aging* 479–495 (2011).

26. Naqvi, S. *et al.* Conservation, acquisition, and functional impact of sex-biased gene expression in mammals. *Science (80-.).* **365**, (2019).

27. Bazhan, N. *et al.* Sex differences in liver, adipose tissue, and muscle transcriptional response to fasting and refeeding in mice. *Cells* **8**, 1529 (2019).

28. Della Torre, S. *et al.* Short-term fasting reveals amino acid metabolism as a major sex-discriminating factor in the liver. *Cell Metab.* **28**, 256–267 (2018).

29. Freire, T. *et al.* Sex-specific metabolic responses to 6 hours of fasting during the active phase in young mice. *J. Physiol.* **598**, 2081–2092 (2020).

30. Tacutu, R. *et al.* Human Ageing Genomic Resources: new and updated databases. *Nucleic Acids Res* **46**, D1083–D1090 (2018).

31. Schartl, M. Beyond the zebrafish: diverse fish species for modeling human disease. *Dis Model Mech* **7**, 181–192 (2014).

32. Podrabsky, J. E., Riggs, C. L. & Wagner, J. T. Tolerance of Environmental Stress. in *Annual Fishes. Life History Strategy, Diversity, and Evolution* (eds. Berois, N., García, G. & De Sá, R. O.) 159–184 (CRC Press, Taylor & Francis, 2016). doi:10.1201/b19016.

33. Jaggard, J. B. *et al.* Cavefish brain atlases reveal functional and anatomical convergence across independently evolved populations. *Sci. Adv.* **6**, eaba3126 (2020).

34. Nielsen, J. *et al.* Eye lens radiocarbon reveals centuries of longevity in the Greenland shark (Somniosus microcephalus). *Science (80-.).* **353**, 702–704 (2016).

35. Kolora, S. R. R. *et al.* Origins and evolution of extreme life span in Pacific Ocean rockfishes. *Science (80-.).* **374**, 842–847 (2021).

36. Vrtílek, M., Žák, J., Pšenička, M. & Reichard, M. Extremely rapid maturation of a wild African annual fish. *Curr. Biol.* **28**, R822–R824 (2018).

37. Harel, I. The turquoise killifish. *Nat. Methods* (2022) doi:10.1038/s41592-022-01631-y.

38. Harel, I. & Brunet, A. The African Turquoise Killifish: A Model for Exploring Vertebrate Aging and Diseases in the Fast Lane. *Cold Spring Harb Symp Quant Biol* (2015) doi:10.1101/sqb.2015.80.027524.

39. Cellerino, A., Valenzano, D. R. & Reichard, M. From the bush to the bench: the annual Nothobranchius fishes as a new model system in biology. *Biol Rev Camb Philos Soc* (2015) doi:10.1111/brv.12183.

40. Platzer, M. & Englert, C. Nothobranchius furzeri: A Model for Aging Research and More. *Trends Genet* **32**, 543–552 (2016).

41. Harel, I. *et al.* A platform for rapid exploration of aging and diseases in a naturally short-lived vertebrate. *Cell* (2015) doi:10.1016/j.cell.2015.01.038.

42. Astre, G., Moses, E. & Harel, I. The African turquoise killifish (Nothobranchius furzeri): biology and research applications. in *Laboratory Fish in Biomedical Research* 245–287 (Elsevier, 2022).

43. Astre, G. *et al.* Genetic perturbation of AMP biosynthesis extends lifespan and restores

metabolic health in a naturally short-lived vertebrate. *Dev. Cell* (2023).

44. Harel, I., Valenzano, D. R. & Brunet, A. Efficient genome engineering approaches for the short-lived African turquoise killifish. *Nat. Protoc.* (2016) doi:10.1038/nprot.2016.103.

45. Reichwald, K. *et al.* Insights into Sex Chromosome Evolution and Aging from the Genome of a Short-Lived Fish. *Cell* **163**, 1527–1538 (2015).

46. Valenzano, D. R. *et al.* The African Turquoise Killifish Genome Provides Insights into Evolution and Genetic Architecture of Lifespan. *Cell* **163**, 1539–1554 (2015).

47. Rozenberg, I., Moses, E. & Harel, I. CRISPR–Cas9 Genome Editing in Nothobranchius furzeri for Gene Knockout and Knock-In. *Cold Spring Harb. Protoc.* (2022).

48. Wang, W. *et al.* Changes in regeneration-responsive enhancers shape regenerative capacities in vertebrates. *Science (80-.).* **369**, (2020).

49. Moses, E., Franek, R. & Harel, I. A scalable and tunable platform for functional interrogation of peptide hormones in fish. *Elife* **12**, e85960 (2023).

50. Slanchev, K., Stebler, J., de la Cueva-Mendez, G. & Raz, E. Development without germ cells: The role of the germ line in zebrafish sex differentiation. *Proc. Natl. Acad. Sci.* (2005) doi:10.1073/pnas.0407475102.

51. Kurokawa, H. *et al.* Germ cells are essential for sexual dimorphism in the medaka gonad. *Proc. Natl. Acad. Sci.* **104**, 16958–16963 (2007).

52. Kossack, M. E. & Draper, B. W. Genetic regulation of sex determination and maintenance in zebrafish (Danio rerio). in *Current topics in developmental biology* vol. 134 119–149 (Elsevier, 2019).

53. Liu, Y. *et al.* Single-cell transcriptome reveals insights into the development and function of the zebrafish ovary. *Elife* **11**, e76014 (2022).

54. Mazutis, L. *et al.* Single-cell analysis and sorting using droplet-based microfluidics. *Nat. Protoc.* **8**, 870–891 (2013).

55. Klein, A. M. *et al.* Droplet barcoding for single-cell transcriptomics applied to embryonic stem cells. *Cell* **161**, 1187–1201 (2015).

56. Sun, X. *et al.* CloneSeq-Single-cell clonal 3D culture and analysis protocol. *STAR Protoc.* **2**, 100794 (2021).

57. Korsunsky, I. *et al.* Fast, sensitive and accurate integration of single-cell data with Harmony. *Nat. Methods* **16**, 1289–1296 (2019).

58. Stévant, I. *et al.* Dissecting cell lineage specification and sex fate determination in gonadal somatic cells using single-cell transcriptomics. *Cell Rep.* **26**, 3272–3283 (2019).

59. Xie, X. *et al.* Single-cell transcriptome profiling reveals neutrophil heterogeneity in homeostasis and infection. *Nat. Immunol.* **21**, 1119–1133 (2020).

60. Chan, J. T. H., Kadri, S., Köllner, B., Rebl, A. & Korytář, T. RNA-Seq of Single Fish Cells–Seeking Out the Leukocytes Mediating Immunity in Teleost Fishes. *Front. Immunol.* **13**, 798712 (2022).

61. Li, L. *et al.* Single-cell RNA-seq analysis maps development of human germline cells and gonadal niche interactions. *Cell Stem Cell* **20**, 858–873 (2017).

62. Estermann, M. A., Major, A. T. & Smith, C. A. Gonadal sex differentiation: Supporting versus steroidogenic cell lineage specification in mammals and birds. *Front. Cell Dev. Biol.* **8**, 1711 (2020).

63. Karlsson, M. *et al.* A single–cell type transcriptomics map of human tissues. *Sci. Adv.* **7**, eabh2169 (2021).

64. Qian, P., Kang, J., Liu, D. & Xie, G. Single cell transcriptome sequencing of Zebrafish testis revealed novel spermatogenesis marker genes and stronger Leydig-germ cell paracrine interactions. *Front. Genet.* **13**, 851719 (2022).

65. Niu, S.-F. *et al.* Characterization of a novel piscidin-like antimicrobial peptide from Pseudosciaena crocea and its immune response to Cryptocaryon irritans. *Fish Shellfish Immunol.* **35**, 513–524 (2013).

66. Yan, T. *et al.* Estradiol Upregulates the Expression of the TGF-β Receptors ALK5 and BMPR2 during the Gonadal Development of Schizothorax prenanti. *Animals* **11**, 1365 (2021).

67. Fan, X. *et al.* Single-cell reconstruction of follicular remodeling in the human adult ovary. *Nat. Commun.* **10**, 3164 (2019).

68. Rotgers, E., Jørgensen, A. & Yao, H. H.-C. At the crossroads of fate—somatic cell lineage specification in the fetal gonad. *Endocr. Rev.* **39**, 739–759 (2018).

69. Yoon, C., Kawakami, K. & Hopkins, N. Zebrafish vasa homologue RNA is localized to the cleavage planes of 2-and 4-cell-stage embryos and is expressed in the primordial germ cells. *Development* **124**, 3157–3165 (1997).

70. Nishimura, T. & Tanaka, M. Gonadal development in fish. *Sex. Dev.* **8**, 252–261 (2014).

71. Schulz, R. W. *et al.* Spermatogenesis in fish. *Gen. Comp. Endocrinol.* **165**, 390–411 (2010).

72. Lubzens, E., Young, G., Bobe, J. & Cerdà, J. Oogenesis in teleosts: how fish eggs are formed. *Gen. Comp. Endocrinol.* **165**, 367–389 (2010).

73. Liu, Y. & Lin, H. Genetic analysis of the reproductive axis in fish using genome-editing nucleases. *Science Bulletin* (2017) doi:10.1016/j.scib.2017.01.002.

74. Li, J. & Cheng, C. H. K. Evolution of gonadotropin signaling on gonad development: Insights from gene knockout studies in zebrafish. *Biology of Reproduction* (2018) doi:10.1093/biolre/ioy101.

75. Zhang, Z., Zhu, B. & Ge, W. Genetic analysis of zebrafish gonadotropin (FSH and LH) functions by TALEN-mediated gene disruption. *Mol. Endocrinol.* (2015) doi:10.1210/me.2014-1256.

76. Chu, L., Li, J., Liu, Y., Hu, W. & Cheng, C. H. K. Targeted gene disruption in zebrafish reveals noncanonical functions of lh signaling in reproduction. *Mol. Endocrinol.* (2014) doi:10.1210/me.2014-1061.

77. Takahashi, A., Kanda, S., Abe, T. & Oka, Y. Evolution of the hypothalamic-pituitary-gonadal axis regulation in vertebrates revealed by knockout medaka. *Endocrinology* (2016) doi:10.1210/en.2016-1356.

78. Chu, L., Li, J., Liu, Y. & Cheng, C. H. K. Gonadotropin signaling in zebrafish ovary and testis development: Insights from gene knockout study. *Mol. Endocrinol.* (2015) doi:10.1210/me.2015-1126.

79. McBride, R. S. *et al.* Energy acquisition and allocation to egg production in relation to fish reproductive strategies. *Fish Fish.* **16**, 23–57 (2015).

80. Williams, T. D. Mechanisms underlying the costs of egg production. *Bioscience* **55**, 39–48 (2005).

81. Lieberman-Aiden, E. *et al.* Comprehensive mapping of long-range interactions reveals folding principles of the human genome. *Science (80-.).* **326**, 289–293 (2009).

82. Durand, N. C. *et al.* Juicer provides a one-click system for analyzing loop-resolution Hi-C experiments. *Cell Syst.* **3**, 95–98 (2016).

83. Rao, S. S. P. *et al.* A 3D map of the human genome at kilobase resolution reveals principles of chromatin looping. *Cell* **159**, 1665–1680 (2014).

84. Weidinger, G. *et al.* dead end, a novel vertebrate germ plasm component, is required for zebrafish primordial germ cell migration and survival. *Curr. Biol.* (2003) doi:10.1016/S0960-9822(03)00537-2.

85. Kedde, M. *et al.* RNA-Binding Protein Dnd1 Inhibits MicroRNA Access to Target mRNA. *Cell* (2007) doi:10.1016/j.cell.2007.11.034.

86. Wargelius, A. *et al.* Dnd knockout ablates germ cells and demonstrates germ cell independent sex differentiation in Atlantic salmon. *Sci. Rep.* **6**, 1–8 (2016).

87. Wendler, S., Hartmann, N., Hoppe, B. & Englert, C. Age-dependent decline in fin regenerative capacity in the short-lived fish Nothobranchius furzeri. *Aging Cell* **14**, 857–866 (2015).

88. Žák, J., Dyková, I. & Reichard, M. Good performance of turquoise killifish (Nothobranchius furzeri) on pelleted diet as a step towards husbandry standardization. *Sci. Rep.* **10**, 8986 (2020).

89. Dyková, I. *et al.* Histology of major organ systems of Nothobranchius fishes: short-lived model species. *J. Vertebr. Biol.* **71**, 21071–21074 (2022).

90. Minchin, J. E. N. & Rawls, J. F. A classification system for zebrafish adipose tissues. *Dis. Model. Mech.* **10**, 797–809 (2017).

91. Orisaka, M., Tajima, K., Tsang, B. K. & Kotsuji, F. Oocyte-granulosa-theca cell interactions during preantral follicular development. *J. Ovarian Res.* **2**, 1–7 (2009).

92. Liu, C., Peng, J., Matzuk, M. M. & Yao, H. H.-C. Lineage specification of ovarian theca cells requires multicellular interactions via oocyte and granulosa cells. *Nat. Commun.* **6**, 1–11 (2015).

93. Koley, S., Rozenbaum, M., Fainzilber, M. & Terenzio, M. Translating regeneration: Local protein synthesis in the neuronal injury response. *Neurosci. Res.* **139**, 26–36 (2019).

94. Zheng, J.-Q. *et al.* A functional role for intra-axonal protein synthesis during axonal regeneration from adult sensory neurons. *J. Neurosci.* **21**, 9291–9303 (2001).

95. Jung, H., Yoon, B. C. & Holt, C. E. Axonal mRNA localization and local protein synthesis in nervous system assembly, maintenance and repair. *Nat. Rev. Neurosci.* **13**, 308–324 (2012).

96. Blanco, S. *et al.* Stem cell function and stress response are controlled by protein synthesis. *Nature* **534**, 335–340 (2016).

97. Riehle, K. J., Dan, Y. Y., Campbell, J. S. & Fausto, N. New concepts in liver regeneration. *J. Gastroenterol. Hepatol.* **26**, 203–212 (2011).

98. Wang, S., Meyer, D. H. & Schumacher, B. H3K4me2 regulates the recovery of protein biosynthesis and homeostasis following DNA damage. *Nat. Struct. Mol. Biol.* **27**, 1165–1177 (2020).

99. Lopez-Otin, C., Blasco, M. A., Partridge, L., Serrano, M. & Kroemer, G. The hallmarks of aging. *Cell* **153**, 1194–1217 (2013).

100. Koyuncu, S. *et al.* Rewiring of the ubiquitinated proteome determines ageing in C. elegans. *Nature* **596**, 285–290 (2021).

101. Tyshkovskiy, A. *et al.* Identification and application of gene expression signatures associated with lifespan extension. *Cell Metab.* **30**, 573–593 (2019).

102. Garratt, M. *et al.* Male lifespan extension with 17-α estradiol is linked to a sex-specific metabolomic response modulated by gonadal hormones in mice. *Aging Cell* **17**, e12786 (2018).

103. Mondal, S. A. *et al.* Metabolic benefits of 17α-estradiol in liver are partially mediated by ERβ in male mice. *Sci. Rep.* **13**, 9841 (2023).

104. Mann, S. N. *et al.* Health benefits attributed to 17α-estradiol, a lifespan-extending compound, are mediated through estrogen receptor α. *Elife* **9**, e59616 (2020).

105. Wink, L., Miller, R. A. & Garcia, G. G. Rapamycin, Acarbose and 17α-estradiol share common mechanisms regulating the MAPK pathways involved in intracellular signaling and inflammation. *Immun. Ageing* **19**, 1–20 (2022).

106. Stout, M. B. *et al.* 17α-Estradiol alleviates age-related metabolic and inflammatory dysfunction in male mice without inducing feminization. *Journals Gerontol. Ser. A Biomed. Sci. Med. Sci.* **72**, 3–15 (2017).

107. Shi, C. & Murphy, C. T. Sex and death. in *Current topics in developmental biology* vol. 144 353–375 (Elsevier, 2021).

108. Wang, C., Li, Q., Redden, D. T., Weindruch, R. & Allison, D. B. Statistical methods for testing effects on "maximum lifespan". *Mech. Ageing Dev.* **125**, 629–632 (2004).

109. Han, S. K. *et al.* OASIS 2: online application for survival analysis 2 with features for the analysis of maximal lifespan and healthspan in aging research. *Oncotarget* **7**, 56147 (2016).

110. Zhao, Y. *et al.* Two forms of death in ageing Caenorhabditis elegans. *Nat. Commun.* **8**, 1–8 (2017).

111. Blencowe, M. *et al.* Relative contributions of sex hormones, sex chromosomes, and gonads to sex differences in tissue gene regulation. *Genome Res.* **32**, 807–824 (2022).

112. Nikkanen, J. *et al.* An evolutionary trade-off between host immunity and metabolism drives fatty liver in male mice. *Science (80-.).* **378**, 290–295 (2022).

113. Garratt, M., Bower, B., Garcia, G. G. & Miller, R. A. Sex differences in lifespan extension with acarbose and 17-α estradiol: gonadal hormones underlie male-specific improvements in glucose tolerance and mTORC 2 signaling. *Aging Cell* **16**, 1256–1266 (2017).

114. Varga, M. *et al.* Autophagy is required for zebrafish caudal fin regeneration. *Cell Death Differ.* **21**, 547–556 (2014).

115. Kozakowska, M., Pietraszek-Gremplewicz, K., Jozkowicz, A. & Dulak, J. The role of oxidative stress in skeletal muscle injury and regeneration: focus on antioxidant enzymes. *J. Muscle Res. Cell Motil.* **36**, 377–393 (2015).

116. Ripa, R. *et al.* Refeeding-associated AMPKγ1 complex activity is a hallmark of health and longevity. *bioRxiv* 2012–2022 (2022).

117. Browning, J. D., Baxter, J., Satapati, S. & Burgess, S. C. The effect of short-term fasting on liver and skeletal muscle lipid, glucose, and energy metabolism in healthy women and men. *J. Lipid Res.* **53**, 577–586 (2012).

118. Zhang, X. *et al.* Fasting induces hepatic lipid accumulation by stimulating peroxisomal dicarboxylic acid oxidation. *J. Biol. Chem.* **296**, (2021).

119. Kramer, D. A., Quiroga, A. D., Lian, J., Fahlman, R. P. & Lehner, R. Fasting and refeeding induces changes in the mouse hepatic lipid droplet proteome. *J. Proteomics* **181**, 213–224 (2018).

120. Meister, A. Glutathione metabolism and its selective modification. *J. Biol. Chem.* **263**, 17205–17208 (1988).

121. Adams, J. D., Lauterburg, B. H. & Mitchell, J. R. Plasma glutathione and glutathione disulfide in the rat: regulation and response to oxidative stress. *J. Pharmacol. Exp. Ther.* **227**, 749–754 (1983).

122. Jenniskens, F. A. *et al.* Effects of fasting on tissue contents of coenzyme A and related intermediates in rats. *Pediatr. Res.* **52**, 437–442 (2002).

123. Lee, M. H., Malloy, C. R., Corbin, I. R., Li, J. & Jin, E. S. Assessing the pentose phosphate

pathway using [2, 3-13C2] glucose. *NMR Biomed.* **32**, e4096 (2019).

124. Bennett, C. F. *et al.* Transaldolase inhibition impairs mitochondrial respiration and induces a starvation-like longevity response in Caenorhabditis elegans. *PLoS Genet.* **13**, e1006695 (2017).

125. Leroi, A. M. Molecular signals versus the Loi de Balancement. *Trends Ecol. Evol.* **16**, 24–29 (2001).

126. Harshman, L. G. & Zera, A. J. The cost of reproduction: the devil in the details. *Trends Ecol. Evol.* **22**, 80–86 (2007).

127. Stearns, S. C. Trade-offs in life-history evolution. *Funct. Ecol.* **3**, 259–268 (1989).

128. Maklakov, A. A. & Chapman, T. Evolution of ageing as a tangle of trade-offs: energy versus function. *Proc. R. Soc. B* **286**, 20191604 (2019).

129. Flatt, T. & Partridge, L. Horizons in the evolution of aging. *BMC Biol.* **16**, 1–13 (2018).

130. Wu, D. *et al.* An antagonistic pleiotropic gene regulates the reproduction and longevity tradeoff. *Proc. Natl. Acad. Sci.* **119**, e2120311119 (2022).

131. Lee, S. D. *et al.* IDOL regulates systemic energy balance through control of neuronal VLDLR expression. *Nat. Metab.* **1**, 1089–1100 (2019).

132. Valenzano, D. R., Terzibasi, E., Cattaneo, A., Domenici, L. & Cellerino, A. Temperature affects longevity and age-related locomotor and cognitive decay in the short-lived fish: Nothobranchius furzeri. *Aging Cell* (2006) doi:10.1111/j.1474-9726.2006.00212.x.

133. Reichard, M. & POLAČIK, M. Reproductive isolating barriers between colour-differentiated populations of an African annual killifish, Nothobranchius korthausae (Cyprinodontiformes). *Biol. J. Linn. Soc.* **100**, 62–72 (2010).

134. Blair, J. A., McGee, H., Bhatta, S., Palm, R. & Casadesus, G. Hypothalamic–pituitary–gonadal axis involvement in learning and memory and Alzheimer's disease: more than "just" estrogen. *Front. Endocrinol. (Lausanne).* **6**, 45 (2015).

135. Udeh-Momoh, C. & Watermeyer, T. Female specific risk factors for the development of Alzheimer's disease neuropathology and cognitive impairment: Call for a precision medicine approach. *Ageing Res. Rev.* **71**, 101459 (2021).

136. Burkewitz, K. *et al.* Neuronal CRTC-1 governs systemic mitochondrial metabolism and lifespan via a catecholamine signal. *Cell* **160**, 842–855 (2015).

137. Smith, H. J., Sharma, A. & Mair, W. B. Metabolic communication and healthy aging: Where should we focus our energy? *Dev. Cell* (2020).

138. Flurkey, K., Papaconstantinou, J. & Harrison, D. E. The Snell dwarf mutation Pit1dw can increase life span in mice. in *Mechanisms of Ageing and Development* (2002). doi:10.1016/S0047-6374(01)00339-6.

139. Flurkey, K., Papaconstantinou, J., Miller, R. A. & Harrison, D. E. Lifespan extension and delayed immune and collagen aging in mutant mice with defects in growth hormone production. *Proc. Natl. Acad. Sci. U. S. A.* (2001) doi:10.1073/pnas.111158898.

140. Bartke, A. & Brown-Borg, H. Life Extension in the Dwarf Mouse. *Curr. Top. Dev. Biol.* (2004) doi:10.1016/S0070-2153(04)63006-7.

141. List, E. O. *et al.* Endocrine parameters and phenotypes of the growth hormone receptor gene disrupted (GHR-/-) mouse. *Endocrine Reviews* (2011) doi:10.1210/er.2010-0009.

142. Aleksic, S. *et al.* Integrity of hypothalamic–pituitary-testicular axis in exceptional longevity. *Aging Cell* e13656 (2022).

143. Harrison, D. E. *et al.* Acarbose, 17-α-estradiol, and nordihydroguaiaretic acid extend mouse

lifespan preferentially in males. *Aging Cell* **13**, 273–282 (2014).

144. Xu, S. *et al.* Estrogen accelerates heart regeneration by promoting the inflammatory response in zebrafish. *J. Endocrinol.* **245**, 39–51 (2020).

145. Losner, J., Courtemanche, K. & Whited, J. L. A cross-species analysis of systemic mediators of repair and complex tissue regeneration. *NPJ Regen. Med.* **6**, 1–11 (2021).

146. Marino, L. & Jornayvaz, F. R. Endocrine causes of nonalcoholic fatty liver disease. *World J. Gastroenterol. WJG* **21**, 11053 (2015).

147. Georgiev, I. P. *et al.* Effects of castration-induced visceral obesity and antioxidant treatment on lipid profile and insulin sensitivity in New Zealand white rabbits. *Res. Vet. Sci.* **90**, 196–204 (2011).

148. Bogdanovitch, S. B. & Man, E. B. The effects of castration, theelin, testosterone and antuitrin-S on the lipoids of blood, liver and muscle of guinea pigs. *Am. J. Physiol. Content* **122**, 73–80 (1938).

149. Zera, A. J. & Harshman, L. G. The physiology of life history trade-offs in animals. *Annu. Rev. Ecol. Syst.* **32**, 95–126 (2001).

150. Wingfield, J. C., Lynn, S. E. & Soma, K. K. Avoiding the ‘costs’ of testosterone: ecological bases of hormone-behavior interactions. *Brain. Behav. Evol.* **57**, 239–251 (2001).

151. Maduro, M. R. & Lamb, D. J. Understanding new genetics of male infertility. *J. Urol.* **168**, 2197–2205 (2002).

152. Kleppe, L. *et al.* Sex steroid production associated with puberty is absent in germ cell-free salmon. *Sci. Rep.* **7**, 1–11 (2017).

153. Siegfried, K. R. & Nüsslein-Volhard, C. Germ line control of female sex determination in zebrafish. *Dev. Biol.* **324**, 277–287 (2008).

154. Habermehl, T. L. *et al.* Extension of longevity and reduction of inflammation is ovarian-dependent, but germ cell-independent in post-reproductive female mice. *GeroScience* **41**, 25–38 (2019).

155. Mason, J. B., Cargill, S. L., Anderson, G. B. & Carey, J. R. Transplantation of young ovaries to old mice increased life span in transplant recipients. *J Gerontol A Biol Sci Med Sci* **64**, 1207–1211 (2009).

156. J.B., M. *et al.* Ovarian-dependent, germ cell-independent extension of longevity and abatement of inflammaging in postreproductive female mice. *GeroScience* (2018) doi:10.1007/s11357-018-0041-z.

157. Toran-Allerand, C. D., Tinnikov, A. A., Singh, R. J. & Nethrapalli, I. S. 17α-Estradiol: a brain-active estrogen? *Endocrinology* **146**, 3843–3850 (2005).

158. Debarba, L. K., Jayarathne, H. S. M., Miller, R. A., Garratt, M. & Sadagurski, M. 17-α-Estradiol has sex-specific effects on neuroinflammation that are partly reversed by gonadectomy. *Journals Gerontol. Ser. A* **77**, 66–74 (2022).

159. Barnes, A. I., Boone, J. M., Jacobson, J., Partridge, L. & Chapman, T. No extension of lifespan by ablation of germ line in Drosophila. *Proc. R. Soc. B Biol. Sci.* **273**, 939–947 (2006).

160. Flatt, T. *et al.* Drosophila germ-line modulation of insulin signaling and lifespan. *Proc. Natl. Acad. Sci.* **105**, 6368–6373 (2008).

161. Astre, G. *et al.* Sex-specific regulation of metabolic health and vertebrate lifespan by AMP biosynthesis. *bioRxiv* 2022.01.10.475524 (2022) doi:10.1101/2022.01.10.475524.

162. Labun, K. *et al.* CHOPCHOP v3: expanding the CRISPR web toolbox beyond genome editing. *Nucleic Acids Res.* **47**, W171–W174 (2019).

163. Jao, L. E., Wente, S. R. & Chen, W. Efficient multiplex biallelic zebrafish genome editing using a CRISPR nuclease system. *Proc Natl Acad Sci U S A* **110**, 13904–13909 (2013).

164. Astre, G., Moses, E. & Harel, I. Laboratory fish in biomedical research. in (eds. D'angelo, L. & de Girolamo, P.).

165. Bavli, D. *et al.* CloneSeq: A highly sensitive analysis platform for the characterization of 3D-cultured single-cell-derived clones. *Dev. Cell* (2021).

166. Alajem, A. *et al.* DNA methylation patterns expose variations in enhancer-chromatin modifications during embryonic stem cell differentiation. *PLoS Genet.* **17**, e1009498 (2021).

167. Li, B. & Dewey, C. N. RSEM: accurate transcript quantification from RNA-Seq data with or without a reference genome. *BMC Bioinformatics* **12**, 1–16 (2011).

168. Langmead, B. & Salzberg, S. L. Fast gapped-read alignment with Bowtie 2. *Nat. Methods* **9**, 357–359 (2012).

169. Wolf, F. A., Angerer, P. & Theis, F. J. SCANPY: large-scale single-cell gene expression data analysis. *Genome Biol.* **19**, 1–5 (2018).

170. Hao, Y. *et al.* Integrated analysis of multimodal single-cell data. *Cell* **184**, 3573–3587 (2021).

171. Yu, G., Wang, L.-G., Han, Y. & He, Q.-Y. clusterProfiler: an R package for comparing biological themes among gene clusters. *Omi. a J. Integr. Biol.* **16**, 284–287 (2012).

172. Carlson, M., Falcon, S., Pages, H. & Li, N. org. Hs. eg. db: Genome wide annotation for Human. *R Packag. version* **3**, (2019).

173. Pagès, H., Carlson, M., Falcon, S. & Li, N. AnnotationDbi: Manipulation of SQLite-based annotations in Bioconductor. R package version1. 54.1. (2021).

174. Andrews, S. FastQC: a quality control tool for high throughput sequence data. 2010. (2017).

175. Ewels, P., Magnusson, M., Lundin, S. & Käller, M. MultiQC: summarize analysis results for multiple tools and samples in a single report. *Bioinformatics* **32**, 3047–3048 (2016).

176. Krueger, F. Trim galore. *A wrapper tool around Cutadapt FastQC to consistently apply Qual. Adapt. trimming to FastQ files* **516**, 517 (2015).

177. Martin, M. Cutadapt removes adapter sequences from high-throughput sequencing reads. *EMBnet. J.* **17**, 10–12 (2011).

178. Dobin, A. *et al.* STAR: ultrafast universal RNA-seq aligner. *Bioinformatics* **29**, 15–21 (2013).

179. McCarthy, D. J., Chen, Y. & Smyth, G. K. Differential expression analysis of multifactor RNA-Seq experiments with respect to biological variation. *Nucleic Acids Res.* **40**, 4288–4297 (2012).

180. Robinson, M. D., McCarthy, D. J. & Smyth, G. K. edgeR: a Bioconductor package for differential expression analysis of digital gene expression data. *Bioinformatics* **26**, 139–140 (2010).

181. Leek, J. T. *Surrogate variable analysis*. (University of Washington, 2007).

182. Gu, Z., Eils, R. & Schlesner, M. Complex heatmaps reveal patterns and correlations in multidimensional genomic data. *Bioinformatics* **32**, 2847–2849 (2016).

183. Carlson, M., Falcon, S., Pages, H. & Li, N. org. Mm. eg. db: Genome wide annotation for Mouse. *R Packag. version* **3**, 10–18129 (2019).

184. Dodzian, J., Kean, S., Seidel, J. & Valenzano, D. R. A Protocol for Laboratory Housing of Turquoise Killifish (Nothobranchius furzeri). *J Vis Exp* (2018) doi:10.3791/57073.

185. Boocholez, H. *et al.* Neuropeptide signaling and SKN-1 orchestrate differential responses of the proteostasis network to dissimilar proteotoxic insults. *Cell Rep.* **38**, (2022).

186. Malitsky, S. *et al.* Viral infection of the marine alga Emiliania huxleyi triggers lipidome remodeling and induces the production of highly saturated triacylglycerol. *New Phytol.* **210**, 88–96 (2016).

187. Salem, M., Bernach, M., Bajdzienko, K. & Giavalisco, P. A simple fractionated extraction method for the comprehensive analysis of metabolites, lipids, and proteins from a single sample. *J. Vis. Exp. JoVE* (2017).

188. Zheng, L. *et al.* Fumarate induces redox-dependent senescence by modifying glutathione metabolism. *Nat. Commun.* **6**, 1–12 (2015).

189. Caspi, R. *et al.* The MetaCyc database of metabolic pathways and enzymes-a 2019 update. *Nucleic Acids Res.* **48**, D445–D453 (2020).

190. Pang, Z. *et al.* MetaboAnalyst 5.0: narrowing the gap between raw spectra and functional insights. *Nucleic Acids Res.* **49**, W388–W396 (2021).

191. Harel, I. *et al.* Distinct origins and genetic programs of head muscle satellite cells. *Dev. Cell* **16**, 822–832 (2009).

192. Harel, I. *et al.* Identification of protein aggregates in the aging vertebrate brain with prion-like and phase separation properties. *bioRxiv* (2022).

193. Gruenbaum-Cohen, Y. *et al.* The actin regulator N-WASp is required for muscle-cell fusion in mice. *Proc. Natl. Acad. Sci.* **109**, 11211–11216 (2012).

194. Theis, S. *et al.* The occipital lateral plate mesoderm is a novel source for vertebrate neck musculature. *Development* **137**, 2961–2971 (2010).

195. Van Keymeulen, A. *et al.* Epidermal progenitors give rise to Merkel cells during embryonic development and adult homeostasis. *J. Cell Biol.* **187**, 91–100 (2009).

196. Benayoun, B. A. *et al.* Remodeling of epigenome and transcriptome landscapes with aging in mice reveals widespread induction of inflammatory responses. *Genome Res* **29**, 697–709 (2019).

197. Harel, I. *et al.* Pharyngeal mesoderm regulatory network controls cardiac and head muscle morphogenesis. *Proc Natl Acad Sci U S A* **109**, 18839–18844 (2012).

198. Longenecker, K. & Langston, R. The jungle histology atlas of gonad stages in coral-reef fishes. *Honolulu, HI Bish. Museum* (2016).

199. Imrie, D. & Sadler, K. C. White adipose tissue development in zebrafish is regulated by both developmental time and fish size. *Dev. Dyn.* **239**, 3013–3023 (2010).

200. Abràmoff, M. D., Magalhães, P. J. & Ram, S. J. Image processing with ImageJ. *Biophotonics Int.* **11**, 36–42 (2004).

201. Hollander-Cohen, L., Golan, M., Aizen, J., Shpilman, M. & Levavi-Sivan, B. Characterization of carp gonadotropins: Structure, annual profile, and carp and zebrafish pituitary topographic organization. *Gen. Comp. Endocrinol.* **264**, 28–38 (2018).

202. Liu, Z. *et al.* Systematic comparison of 2A peptides for cloning multi-genes in a polycistronic vector. *Sci. Rep.* **7**, 1–9 (2017).

Figure 1

a. Experimental design

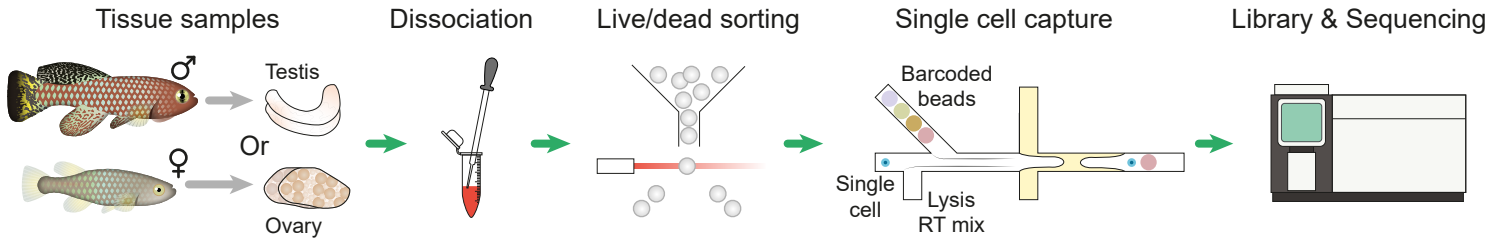

b. UMAP plots for gonadal cell types

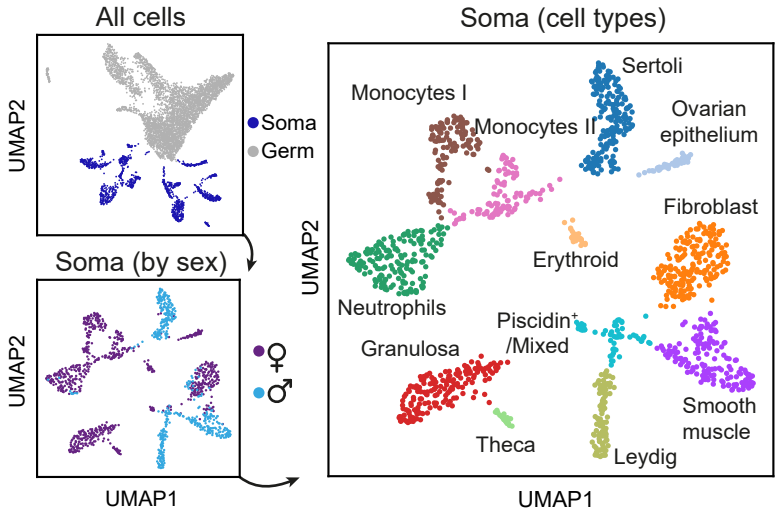

c. Dot-plot for select marker genes

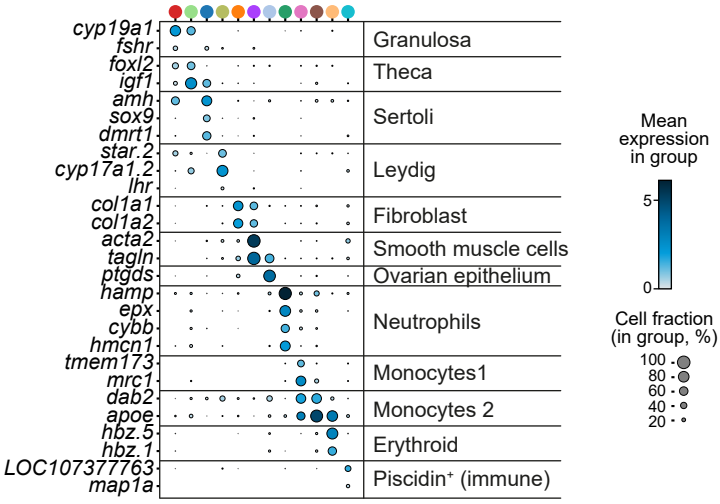

d. UMAP plots of select marker genes.

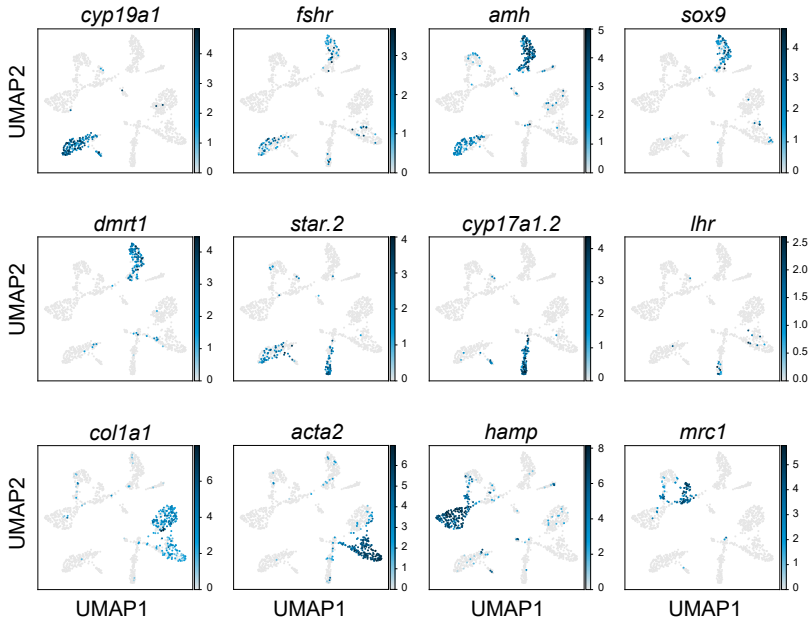

e. Single-molecule FISH for selected markers

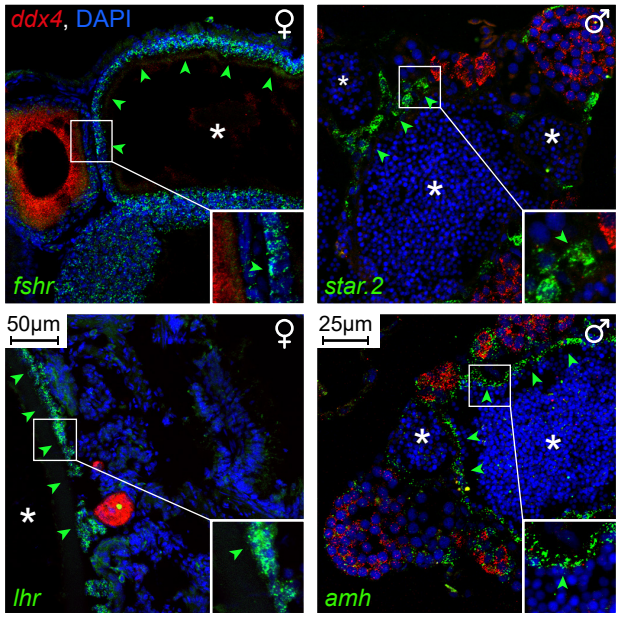

f. Gonad structure and marker genes for primary cell types in males and females

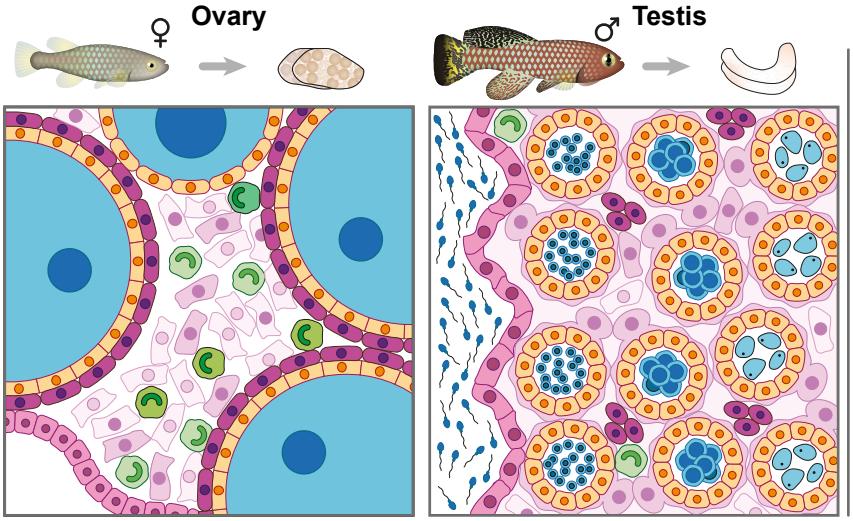

Cell type	Ovary	Testis
Supporting:	Granulosa *cyp19a1, fshr*	Sertoli *amh, sox9, dmrt1*
Steroidogenic:	Theca *foxl2, igf1*	Leydig *star.2, lhr*
Germ cells: (immature)	Oocyte *ddx4*	Sperm *ddx4*
Stromal cells (fibroblast): *col1a1, col1a2*		Neutrophils: *hamp, epx*
Myoid cells (smooth muscle): *acta2, tagln*		Monocytes 1: *tmem173, mrc1*
Ovarian epithelium: *ptgds*		Monocytes 2: *apoe*

Figure 2

a. The hypothalamic–pituitary–gonadal (HPG) reproductive axis in vertebrates

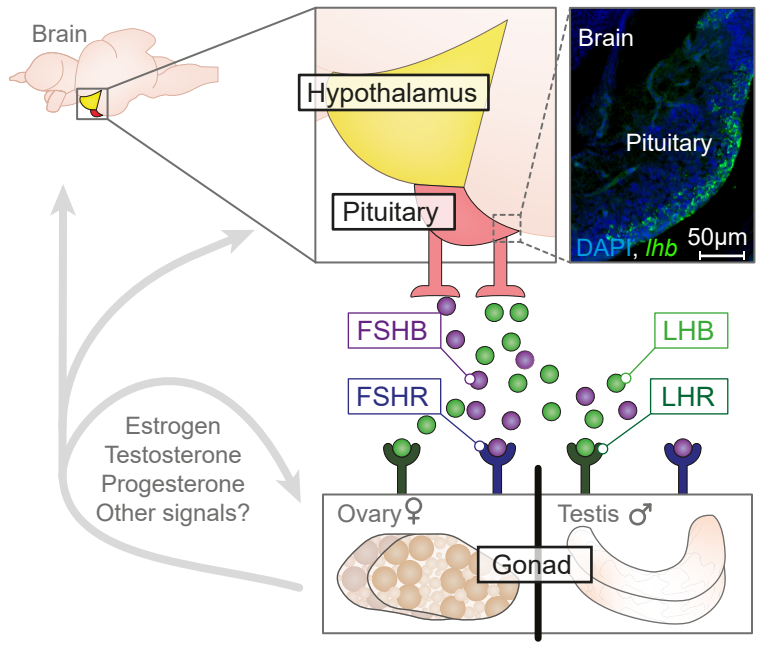

b. CRISPR mutants for HPG axis

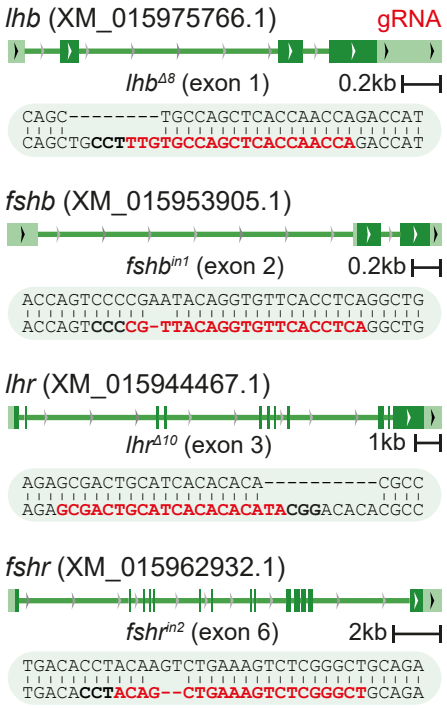

c. Histology of ovaries in HPG female mutants

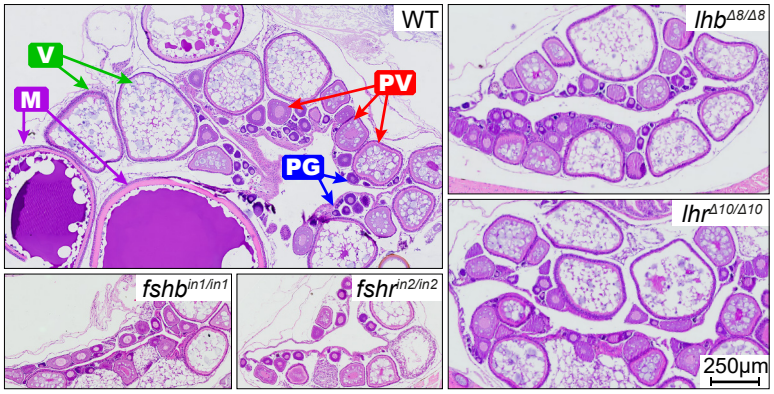

d. Oocyte maturation in HPG female mutants

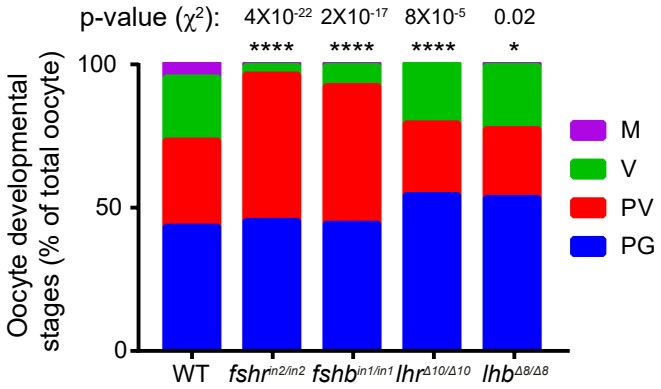

e. Fertility of HPG female mutants

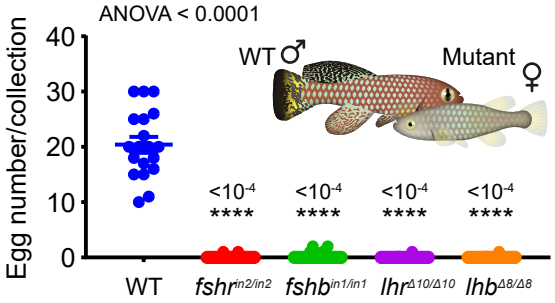

f. The HPG axis regulates killifish ovary development

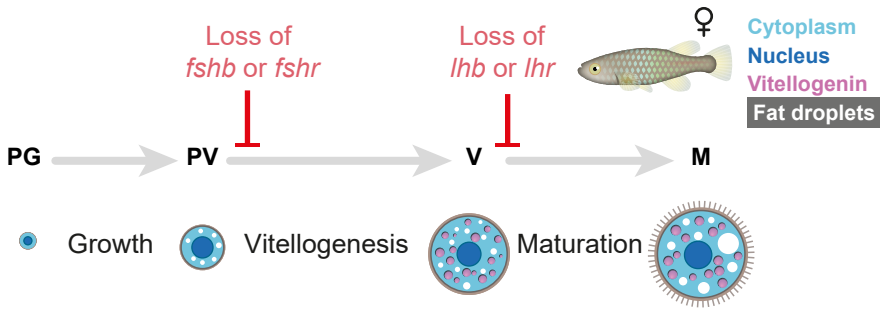

g. Chromosome conformation capture (Hi-C) places *lhb* in proximity to the sex locus

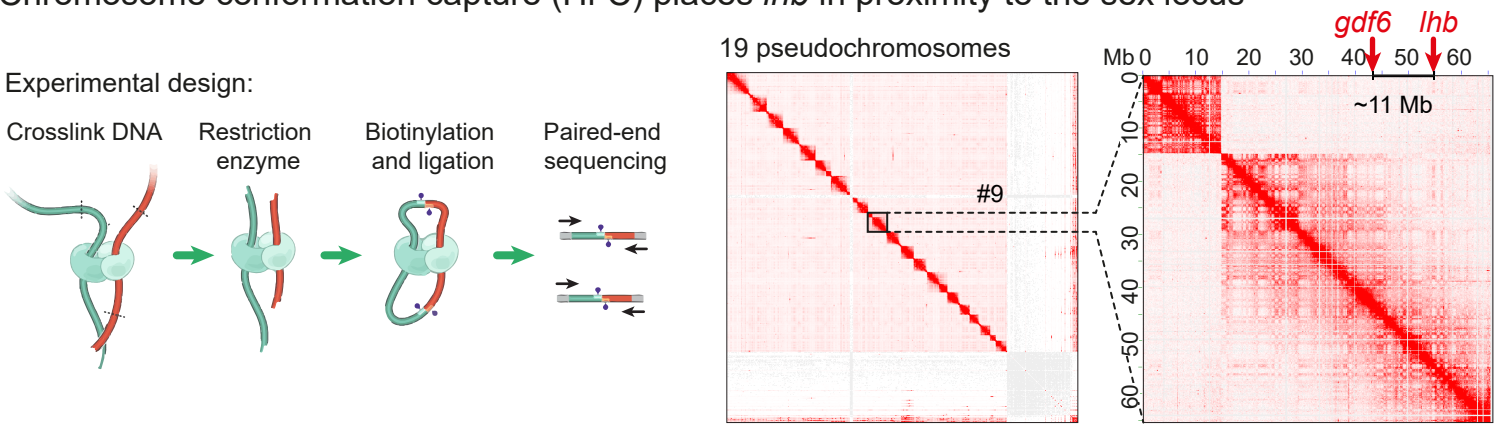

Figure 3

a. Germline depletion in *dnd1*$^{\Delta4/\Delta4}$ male and female mutants

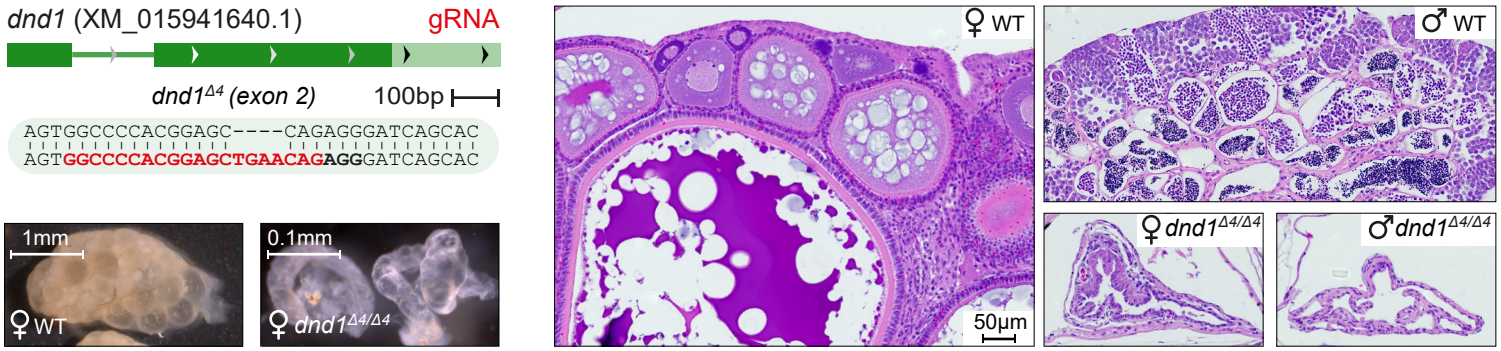

b. Experimental design

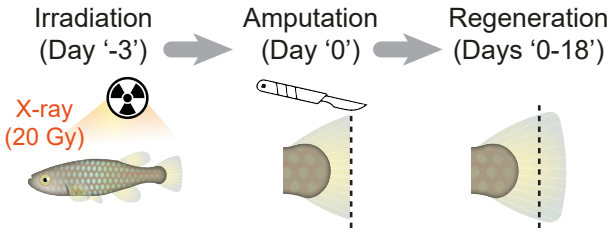

c. Tail regeneration of WT fish at day 18

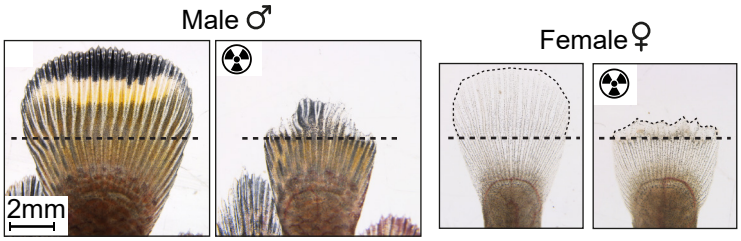

d. Tail regeneration in germline depleted females following whole-body irradiation

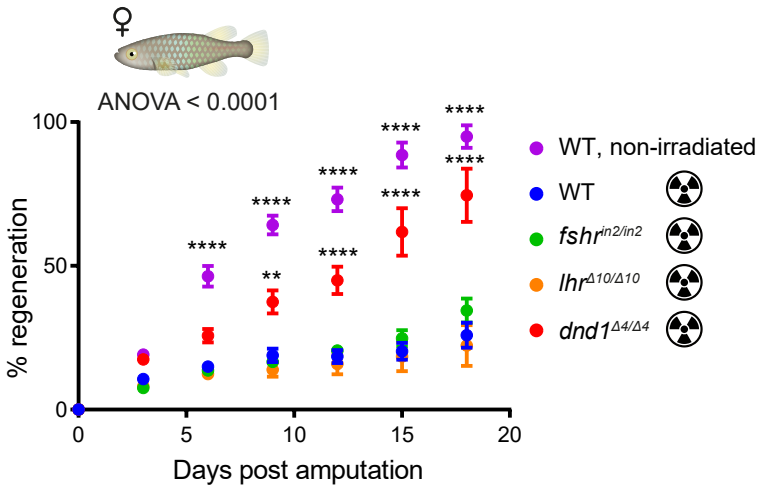

e. Distinct reproductive states affect female tail regeneration following irradiation

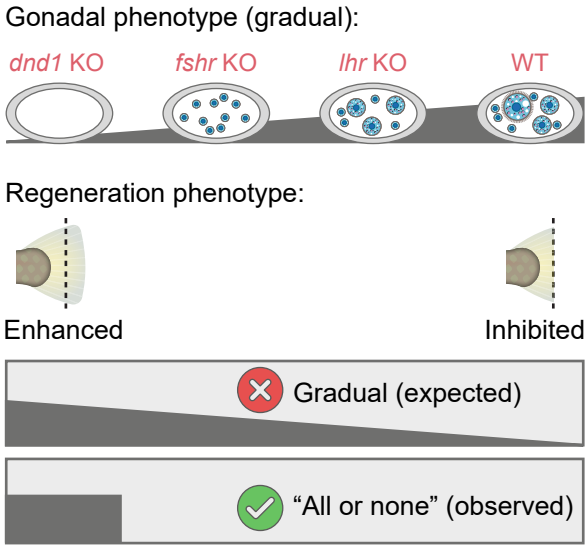

Figure 4

a. UMAP plots for gonadal cell types

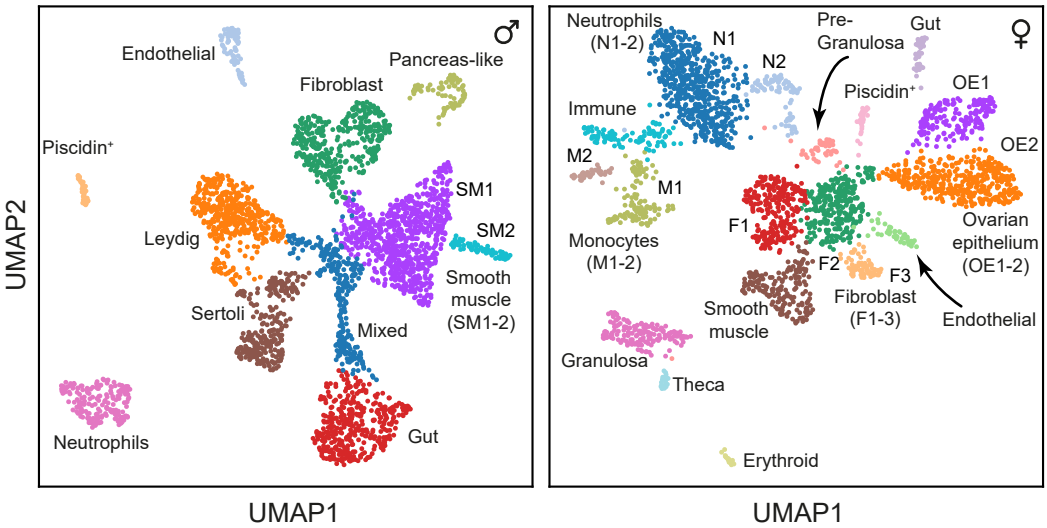

b. smFISH for marker genes in *dnd1*$^{\Delta4/\Delta4}$ gonads

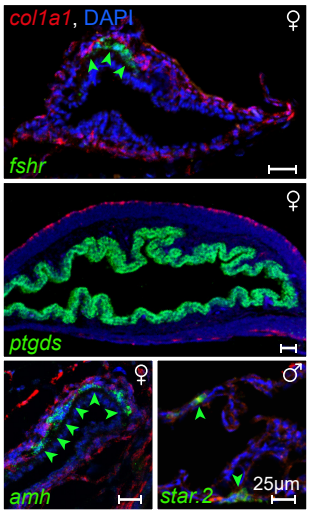

c. GO enrichment analysis for upregulated genes in *dnd1*$^{\Delta4/\Delta4}$ gonadal cell types

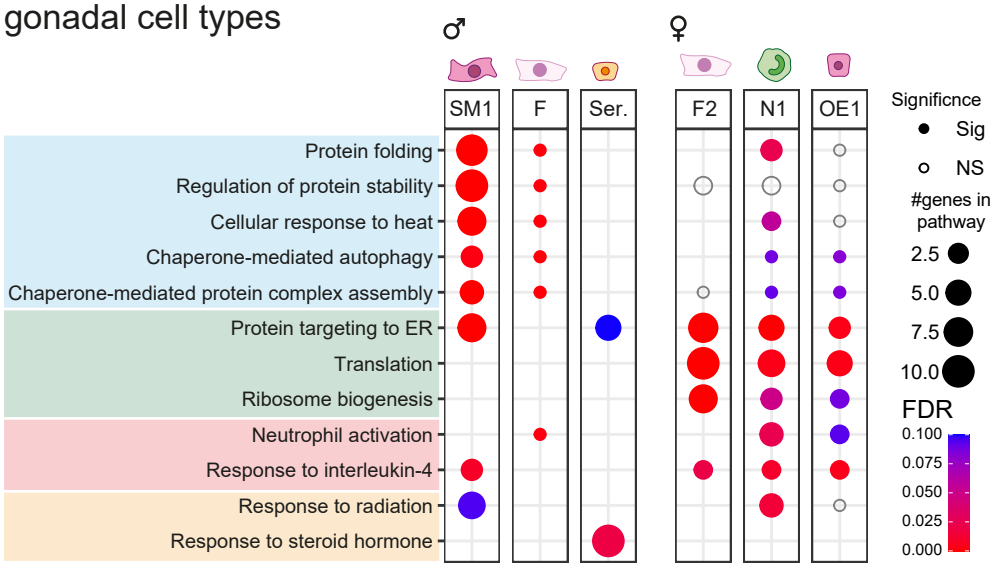

d. smFISH for marker genes in *dnd1*$^{\Delta4/\Delta4}$ gonad and gut

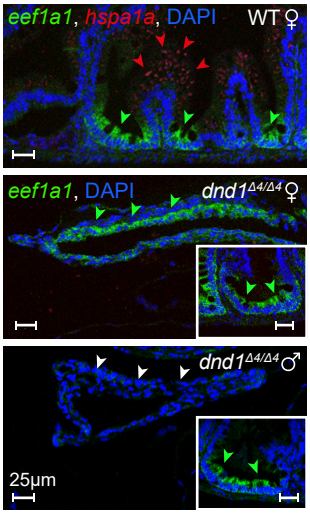

Figure 5

a. Comparing the hepatic transcriptional response of young *dnd1*$^{\Delta4/\Delta4}$ killifish mutants with common lifespan-extending interventions in mice

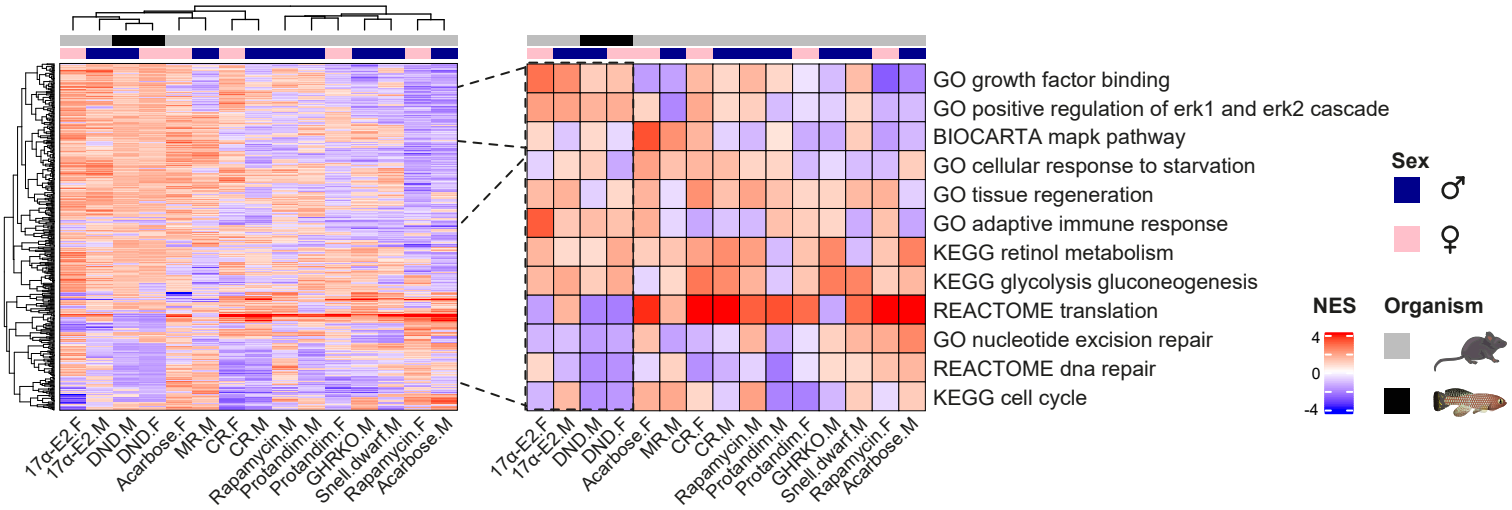

b. Lifespan of WT and *dnd1*$^{\Delta4/\Delta4}$ fish

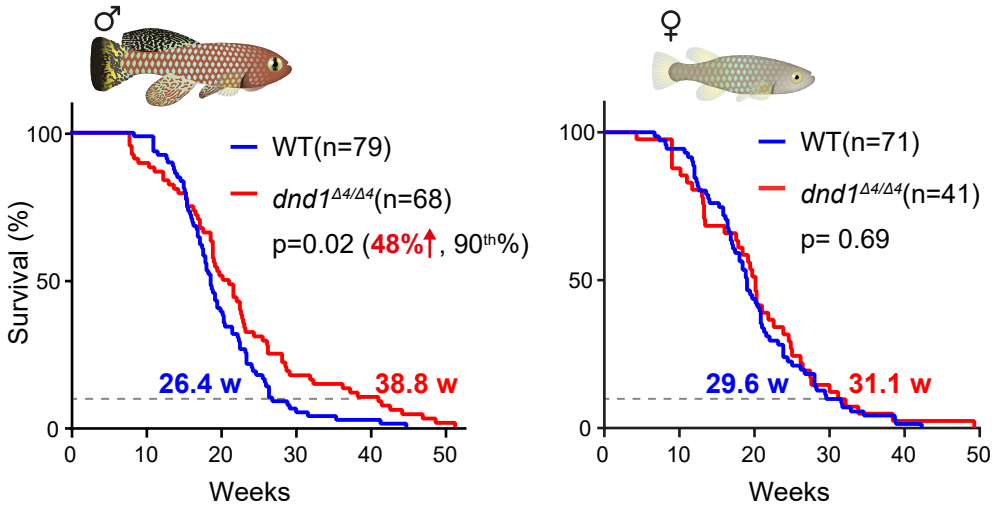

c. Sexually dimorphic effects of germline ablation

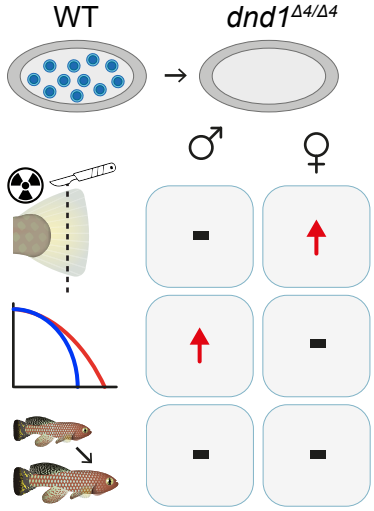

Figure 6

a. Hepatic gene expression following germline depletion in male and female killifish

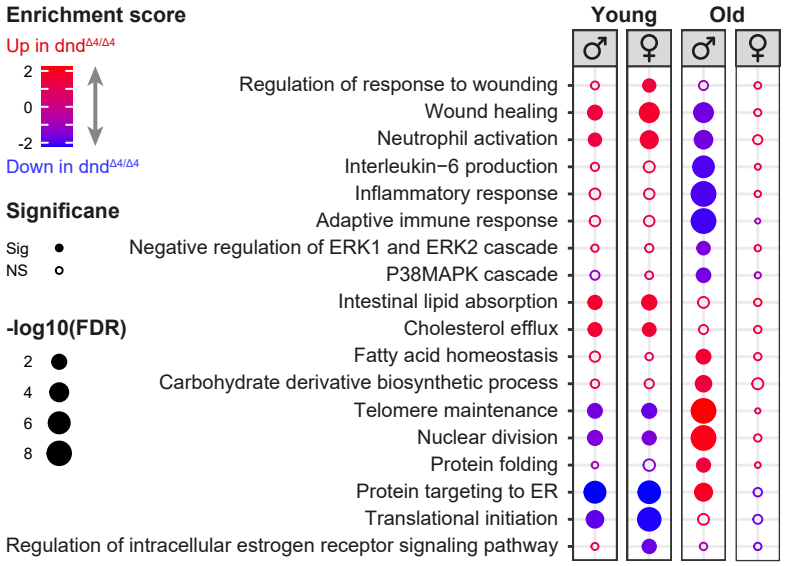

b. Age- and sex-dependent transcriptional response to the *dnd1*$^{\Delta4/\Delta4}$ mutation

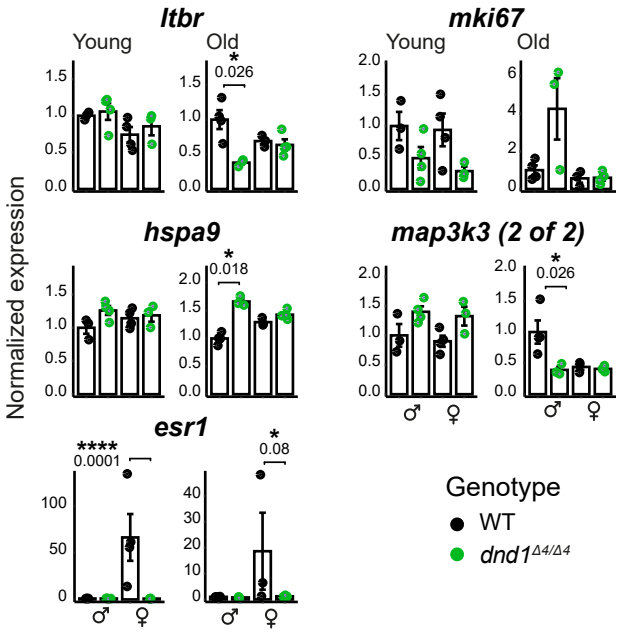

c. Male blood glucose at metabolic baseline

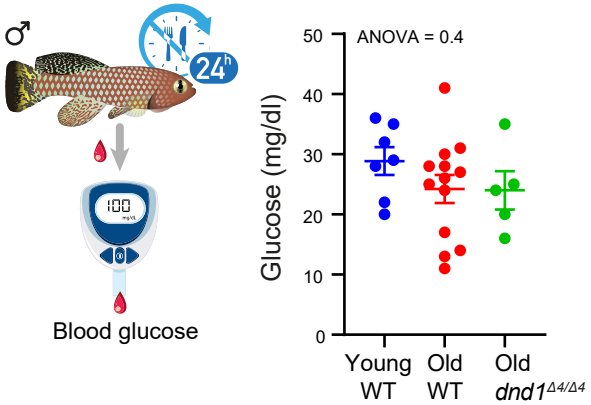

d. 'Young-like' liver histology in old mutant males

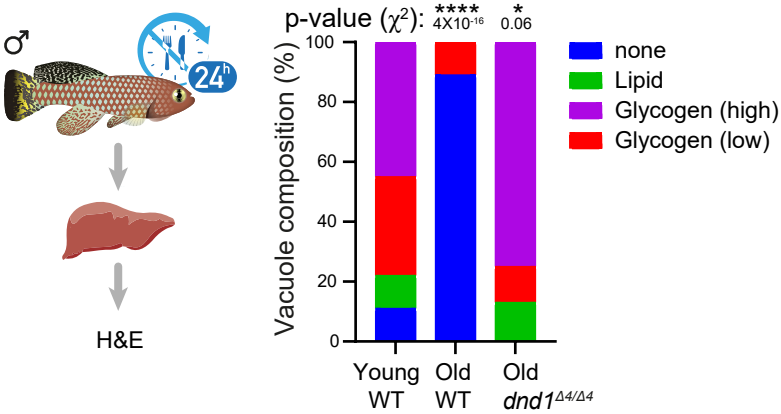

e. PCA for liver metabolites in old males

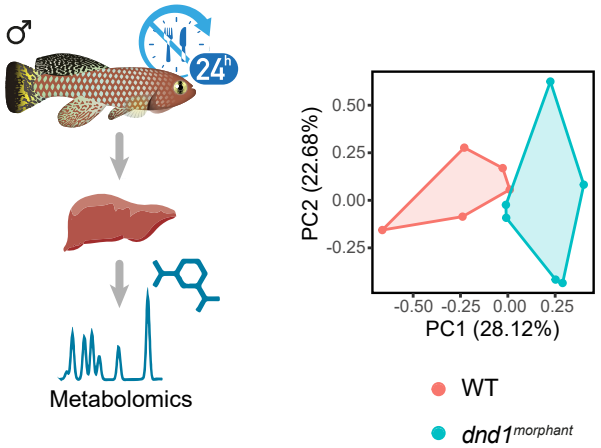

f. Significantly alterd liver metabolites in old males

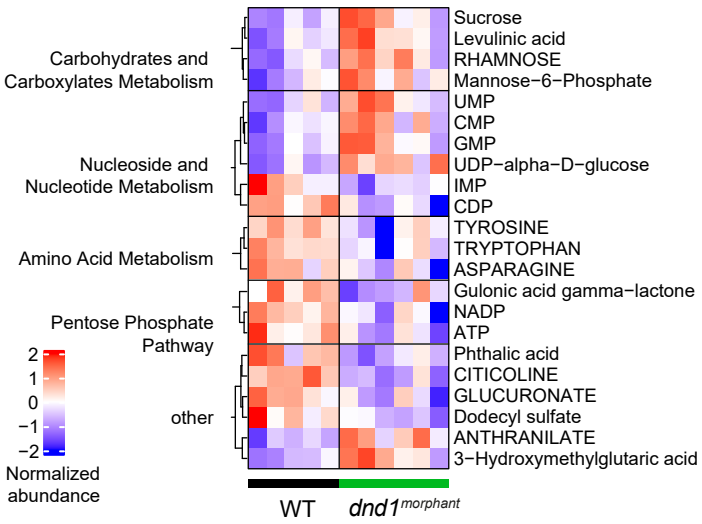

Figure S1

a. A UMAP plot of a germline marker

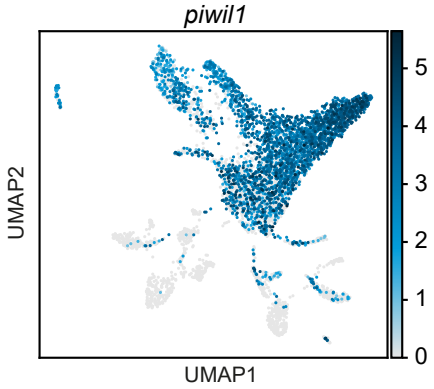

b. Cluster analysis for germ cell populations

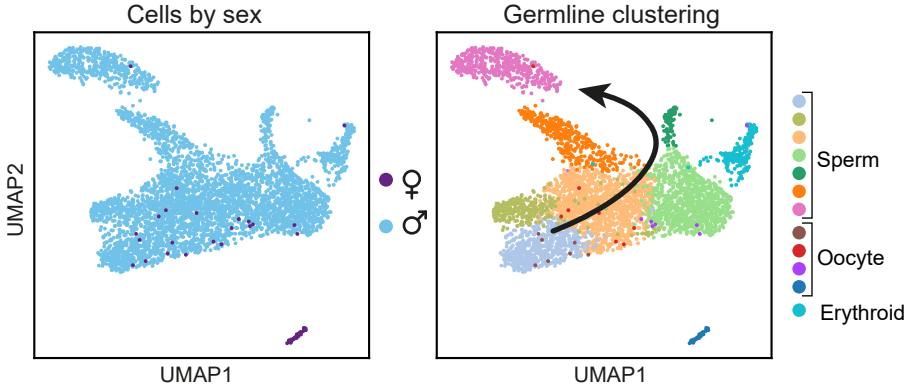

c. Dot-plot for selected marker genes

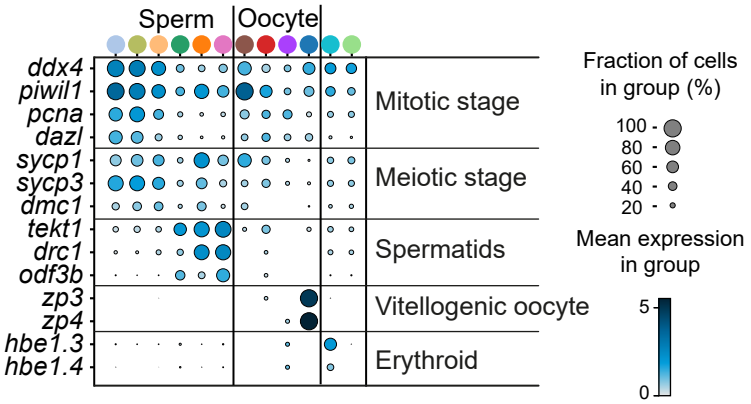

d. UMAP plots of select marker genes

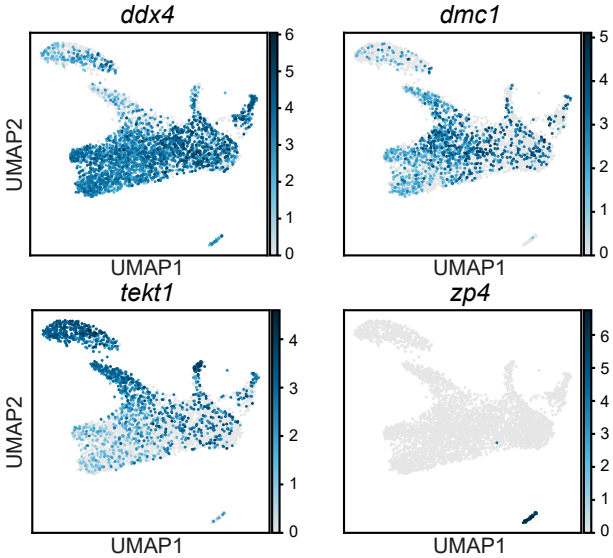

e. Evolutionary conservation of germ and somatic cell markers

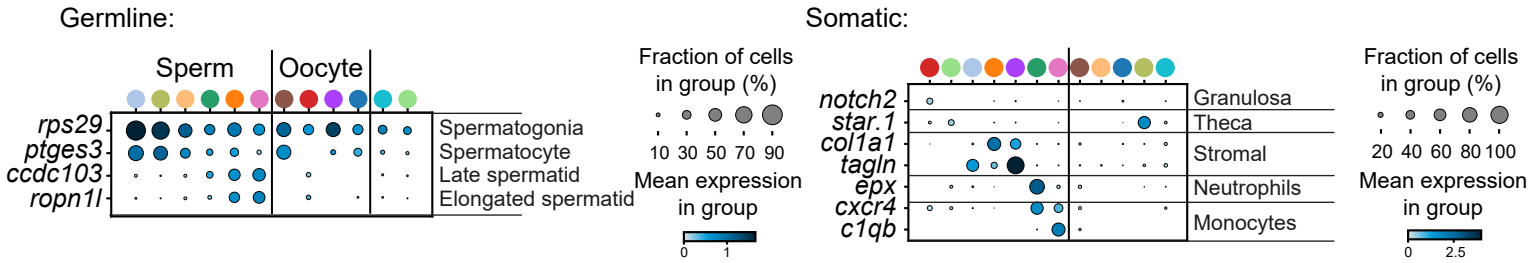

f. Developmental trajectory of male germ cells

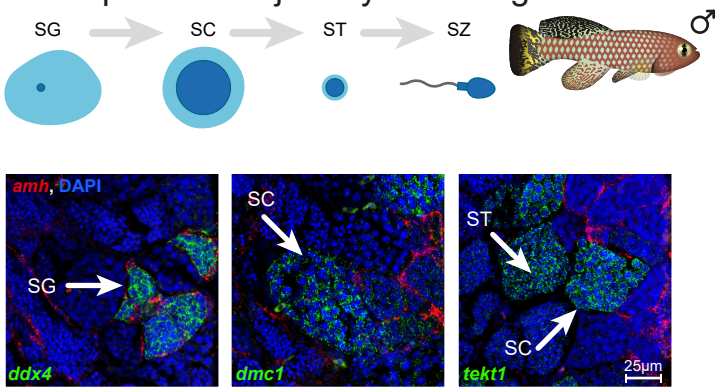

g. Developmental trajectory of female germ cells

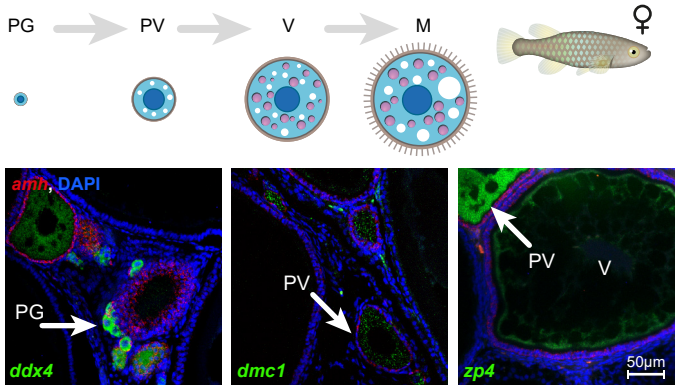

Figure S2

a. Histology of the testis in HPG male mutants

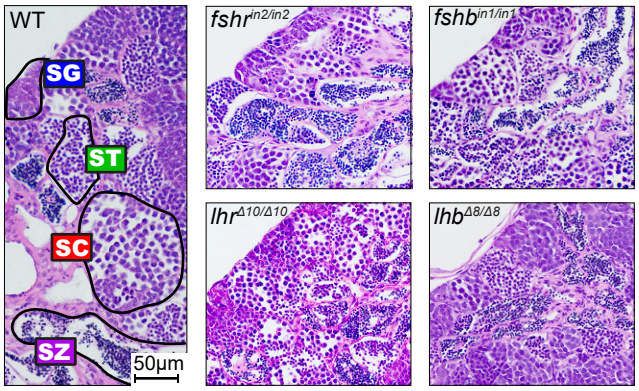

b. Sperm maturation in HPG male mutants

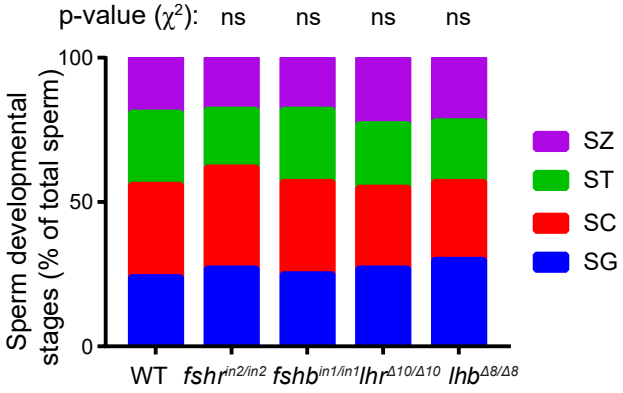

c. Genotype proportions

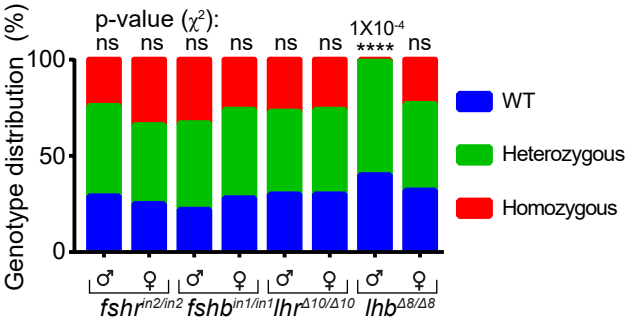

d. Size of HPG male and female mutants at maturity

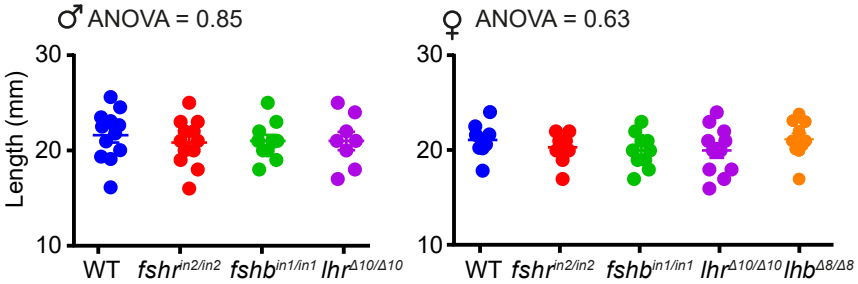

e. Fertility of HPG male mutants

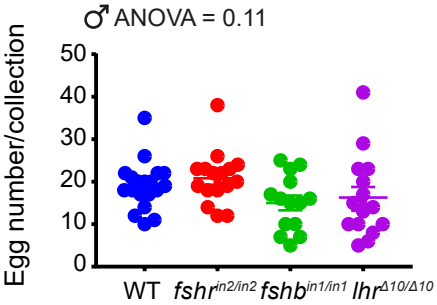

f. Rescue of female fertility defects in *lhb*$^{\Delta 8/\Delta 8}$ mutants

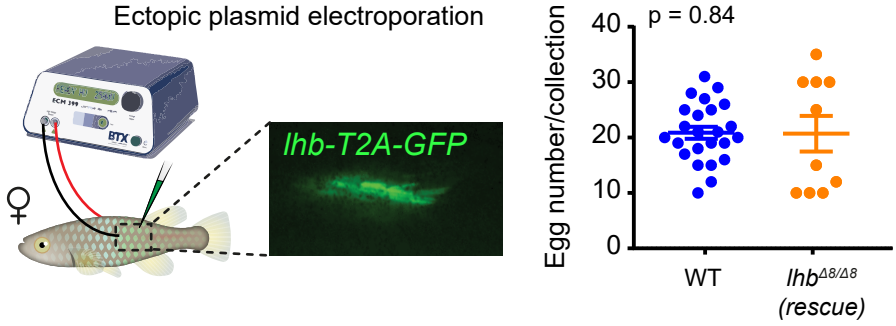

g. smFISH for receptor mutants in females

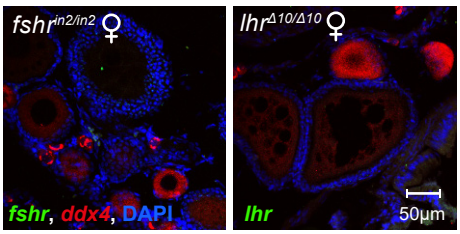

h. Hi-C scaffolded assembly

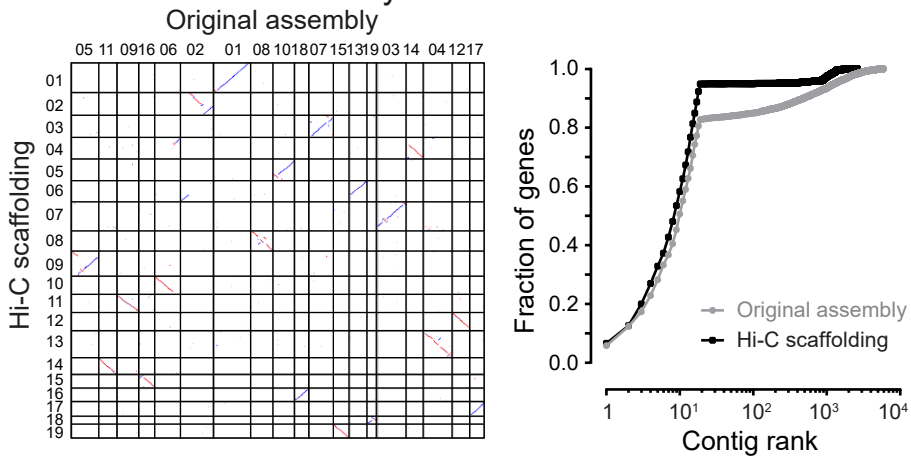

Figure S3

a. Length at maturity of *dnd1*$^{\Delta4/\Delta4}$ mutants

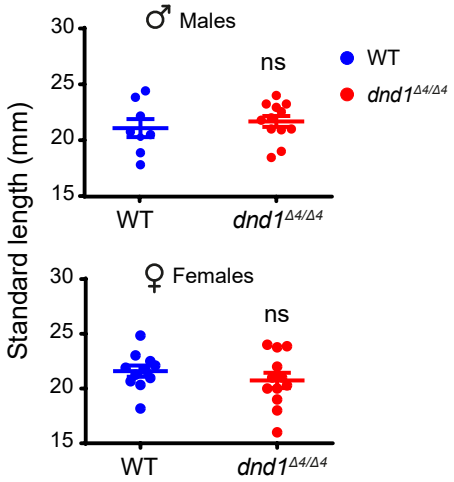

b. Adult *dnd1*$^{\Delta4/\Delta4}$ fish

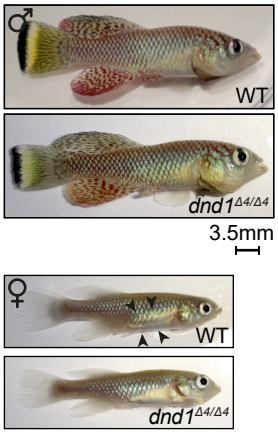

c. Stratified *dnd1*$^{\Delta4/\Delta4}$ mutants by sex and genotype

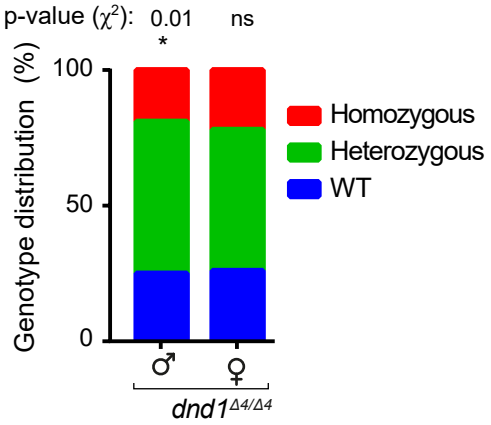

d. Tail regeneration in males following whole-body irradiation

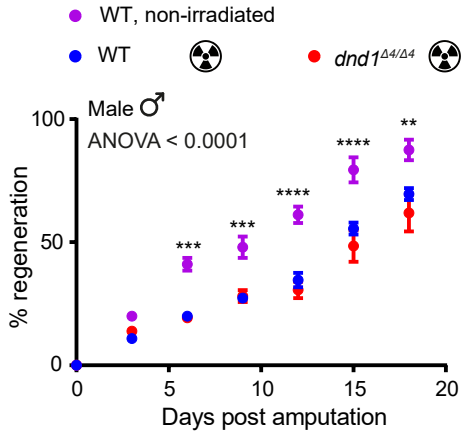

e. Tail regeneration in non-irradiated WT and *dnd1*$^{\Delta4/\Delta4}$ fish of both sexes during aging

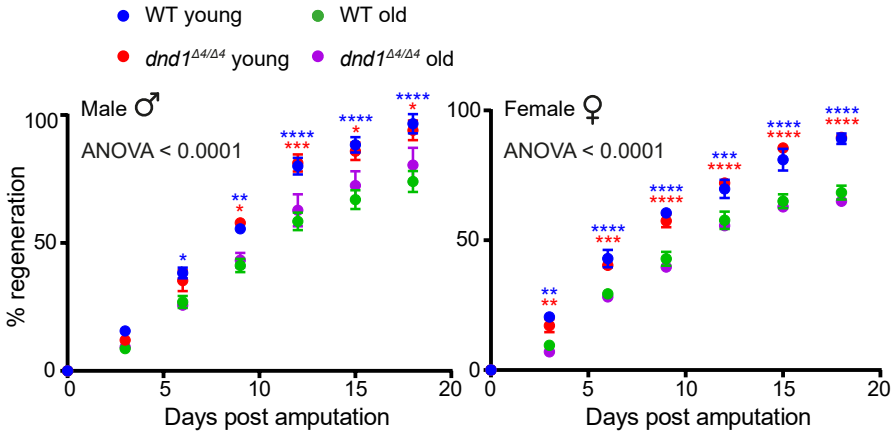

f. Apoptosis following either whole-body or tail-specific irradiation

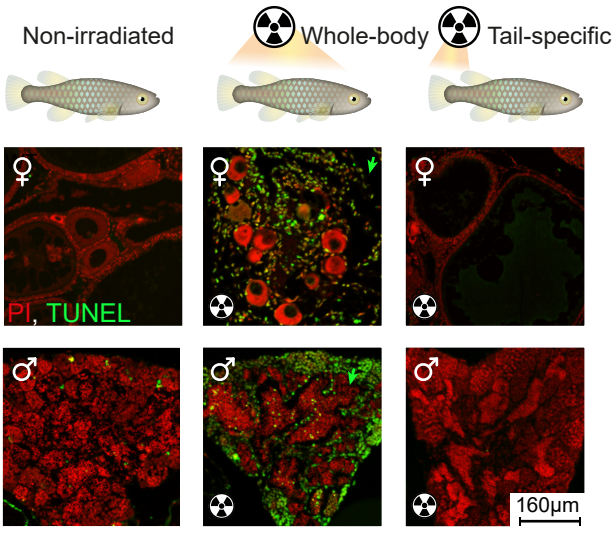

g. Tail regeneration following whole-body or tail-specific irradiation

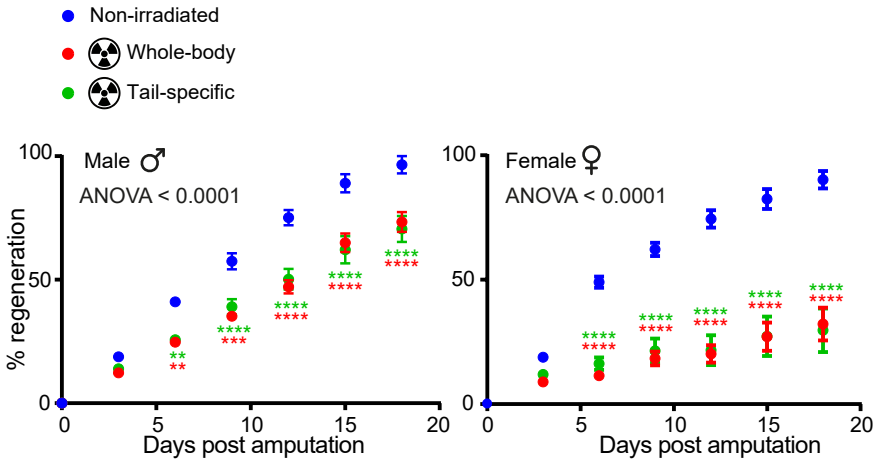

h. H&E for liver and adipose tissue

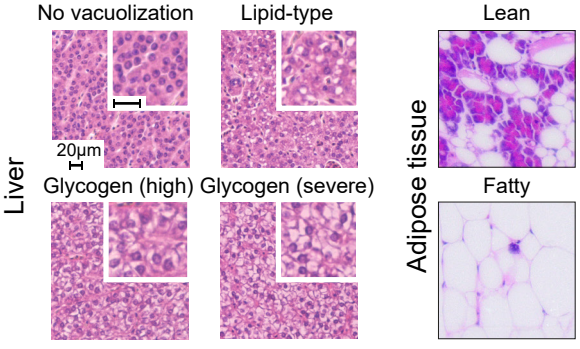

i. Hepatic vacuoles in germline-depleted fish

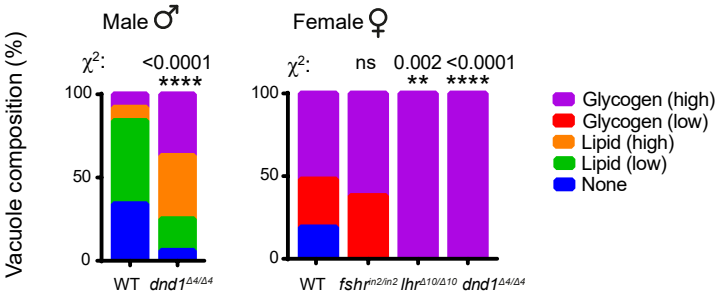

Figure S4

a. UMAP plots for gonadal cells by genotype

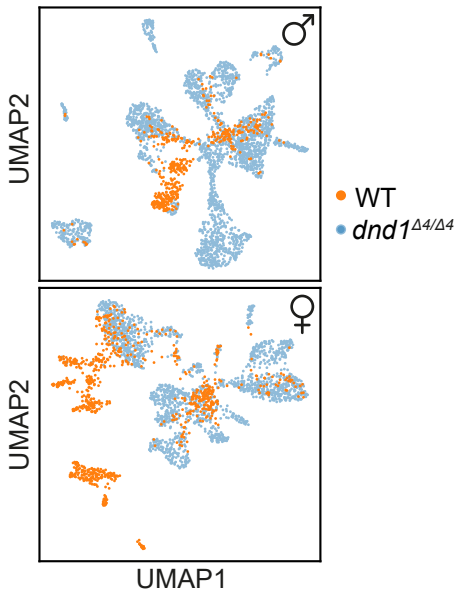

b. Dot-plot and UMAP plots for select marker genes in males

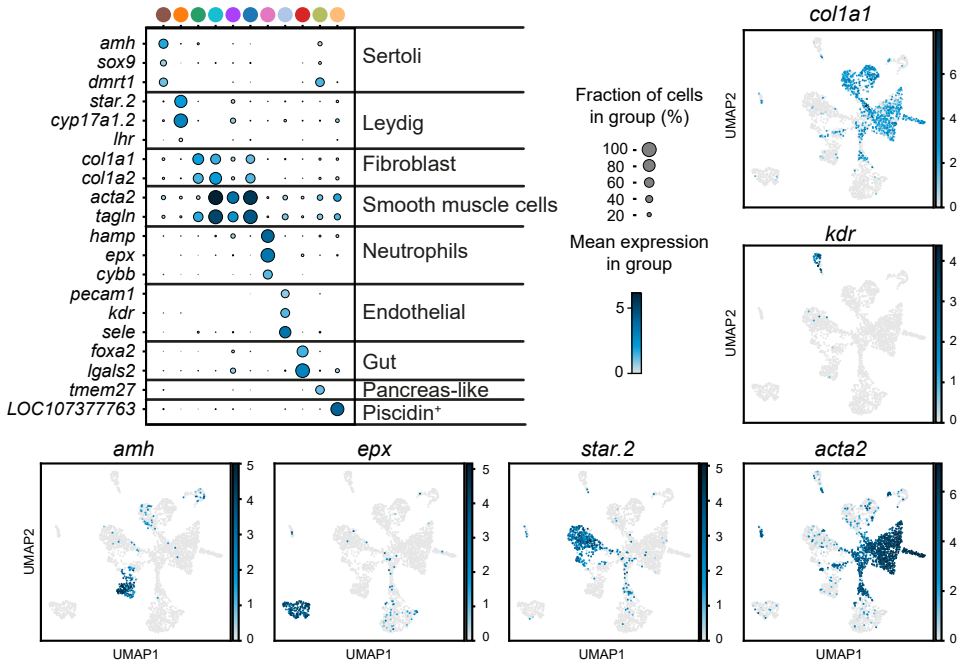

c. Dot-plot and UMAP plots for select marker genes in females

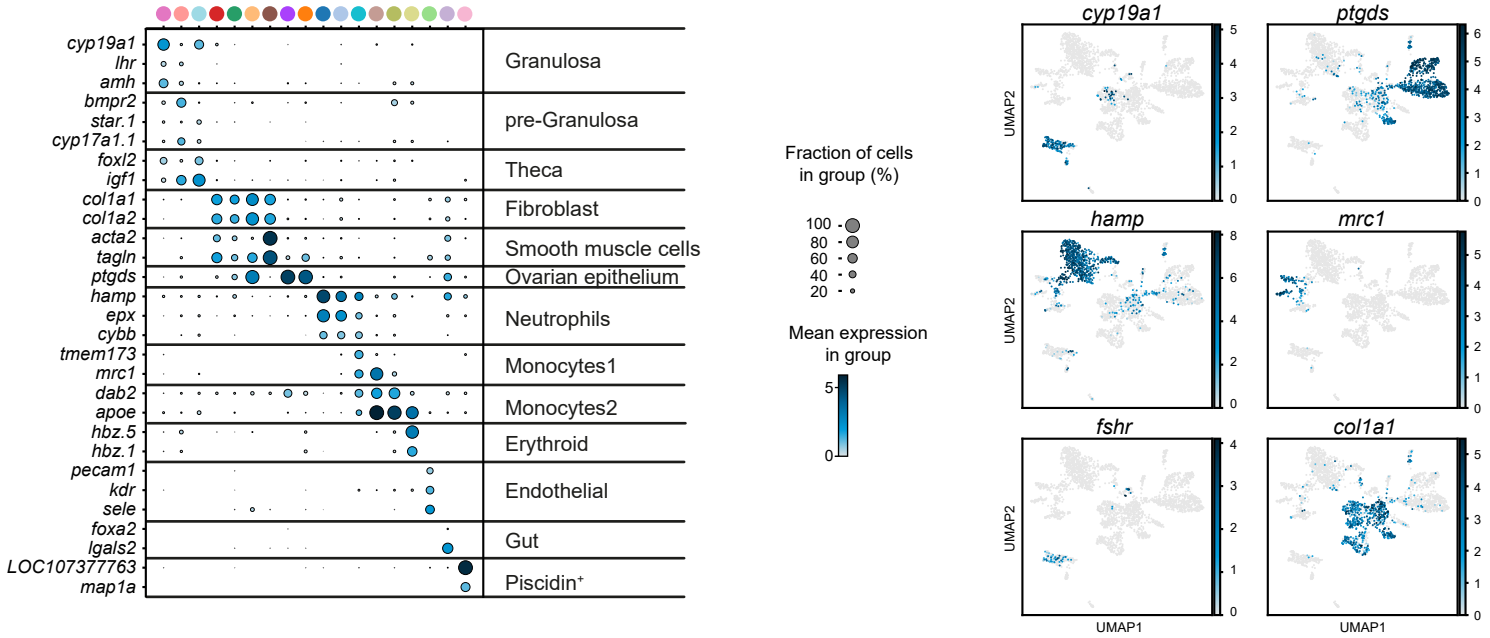

d. smFISH for markers for pre- and mature Granulosa in *dnd1*$^{\Delta4/\Delta4}$ female gonads

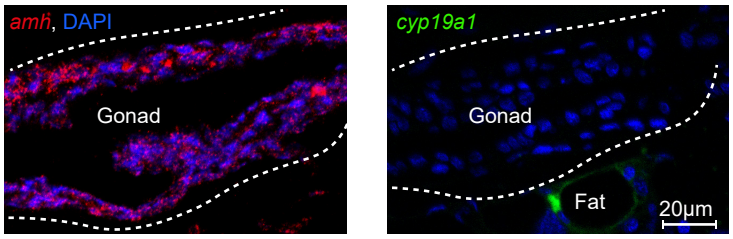

e. Selected driver genes

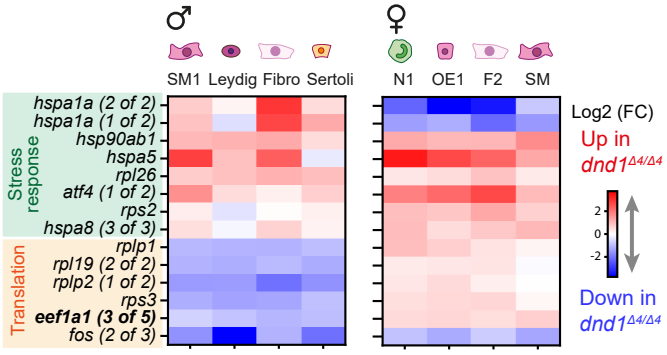

f. smFISH in WT and *dnd1*$^{\Delta4/\Delta4}$ ovary

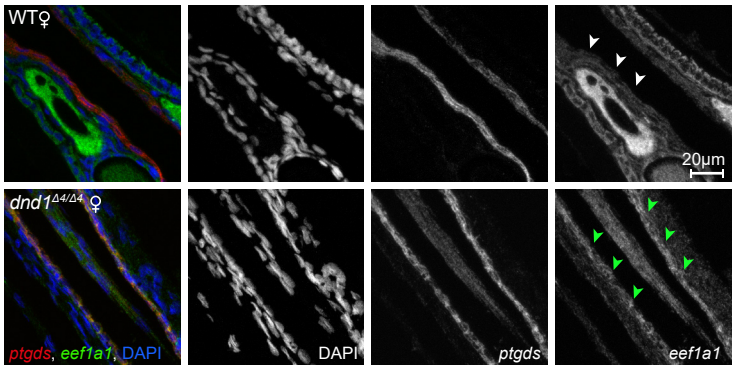

Figure S5

a. Quantile-Quantile (Q-Q) plot for the lifespan data of WT and *dnd1*$^{\Delta4/\Delta4}$ fish

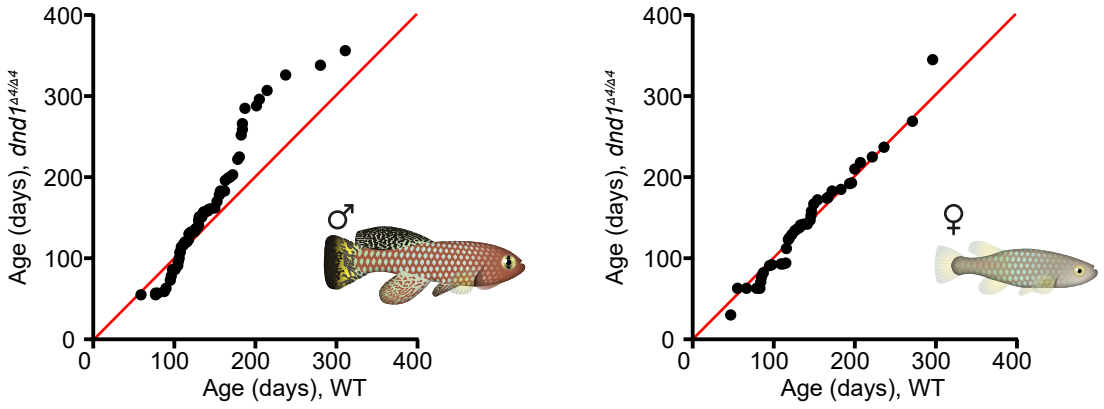

b. Pathway enrichment analysis, comparing the transcriptional response of male *dnd1*$^{\Delta4/\Delta4}$ young killifish with gonadal and hormonal interventions in male mice

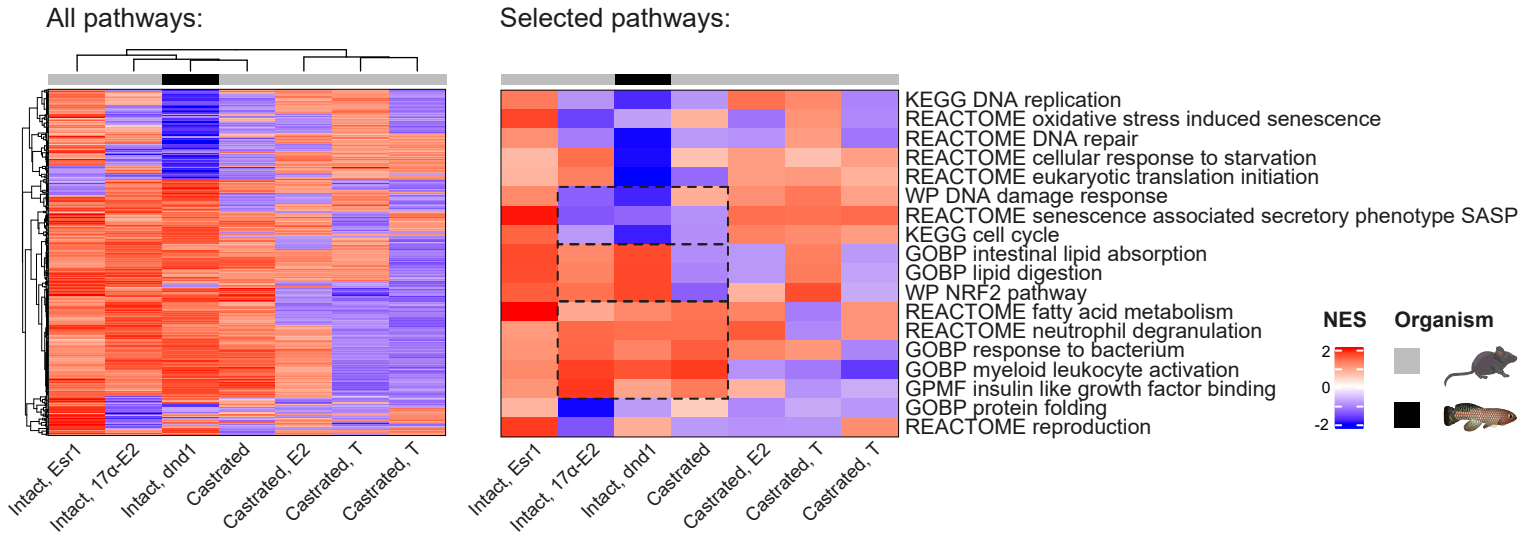

c. Testing candidate genes from killifish as longevity modifiers in germline-depleted worms

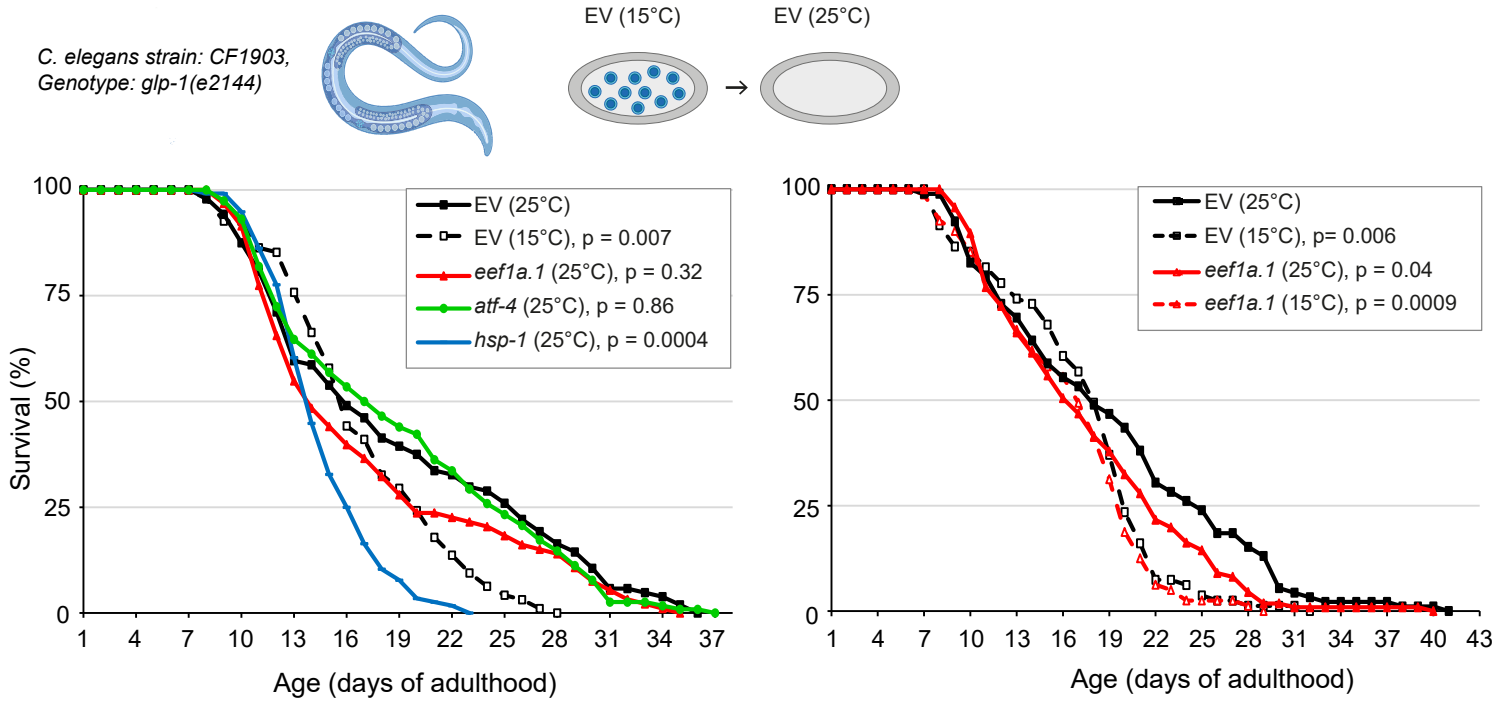

Figure S6

a. PCA RNA seq

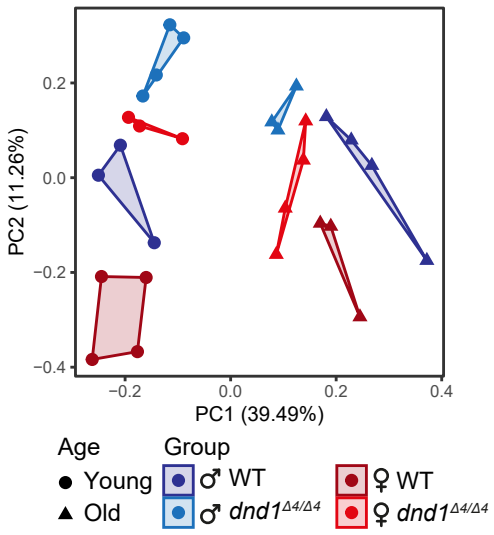

b. Tail regeneration in *dnd1*^{morphant} following whole-body irradiation

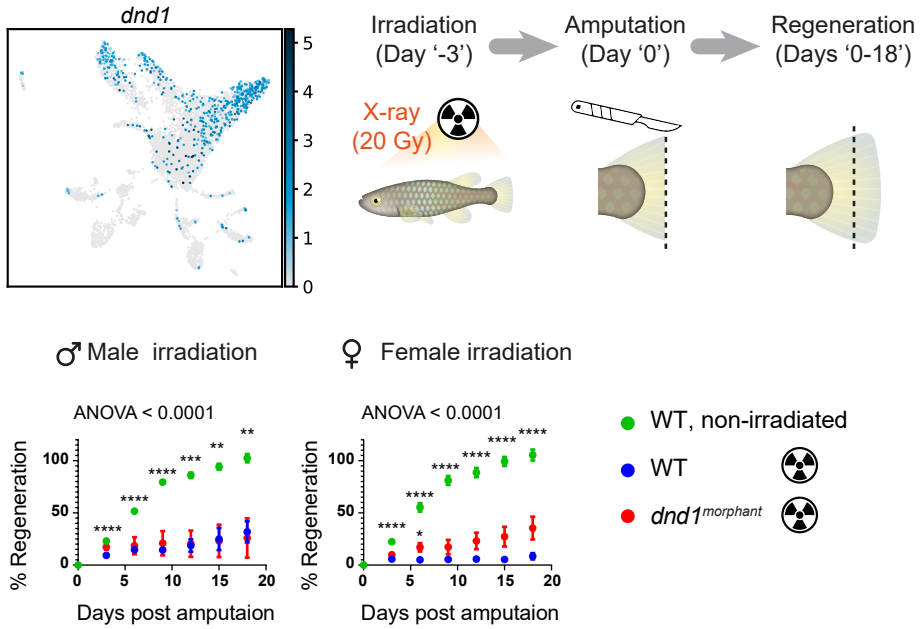

c. Tail regeneration is inhibited in WT fish following exposure to chloroquine or paraquat

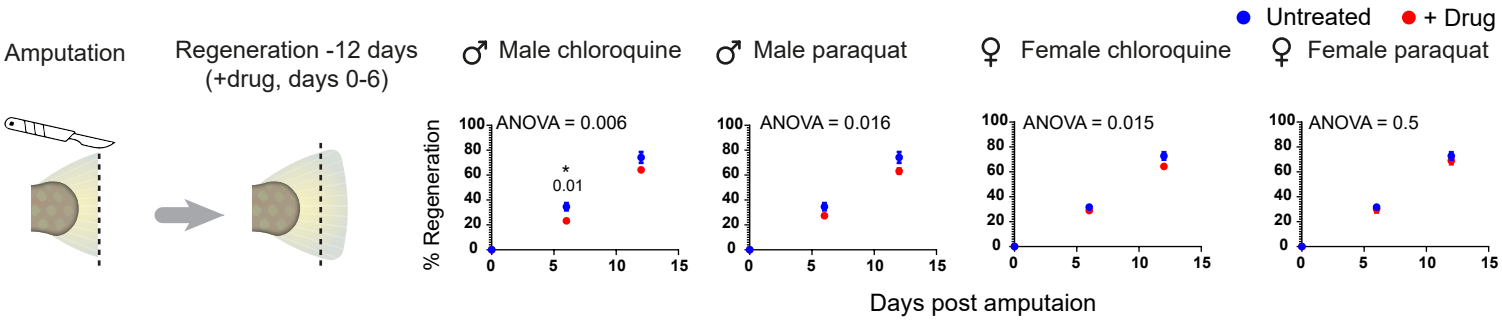

d. Tail regeneration in *dnd1*^{morphant} following exposure to different stressors

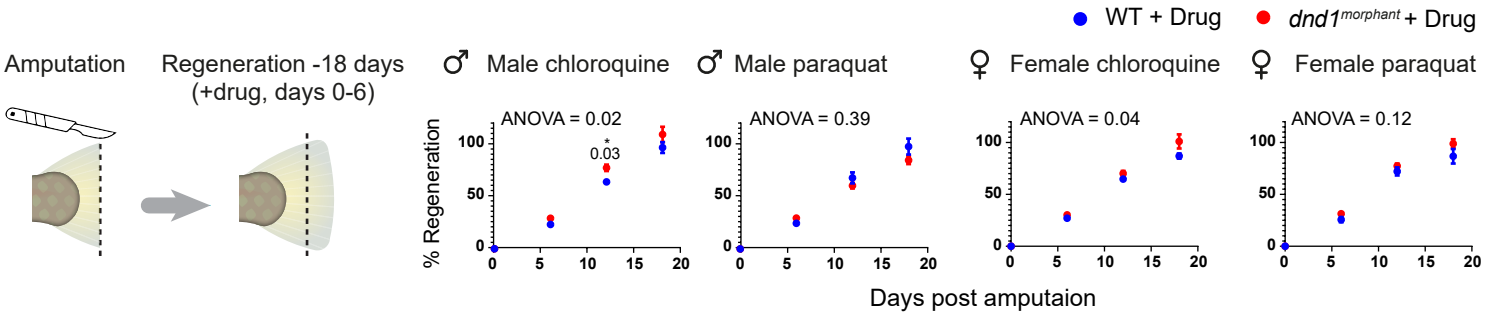
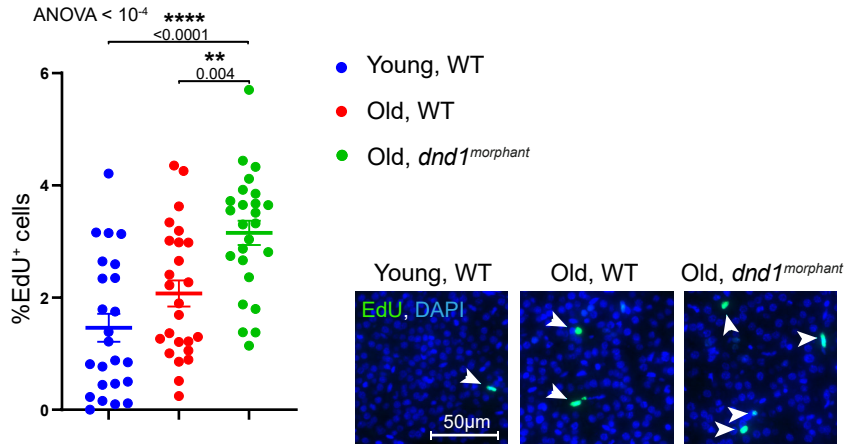
e. Hepatic cell proliferation in *dnd1*^{morphant} male fish